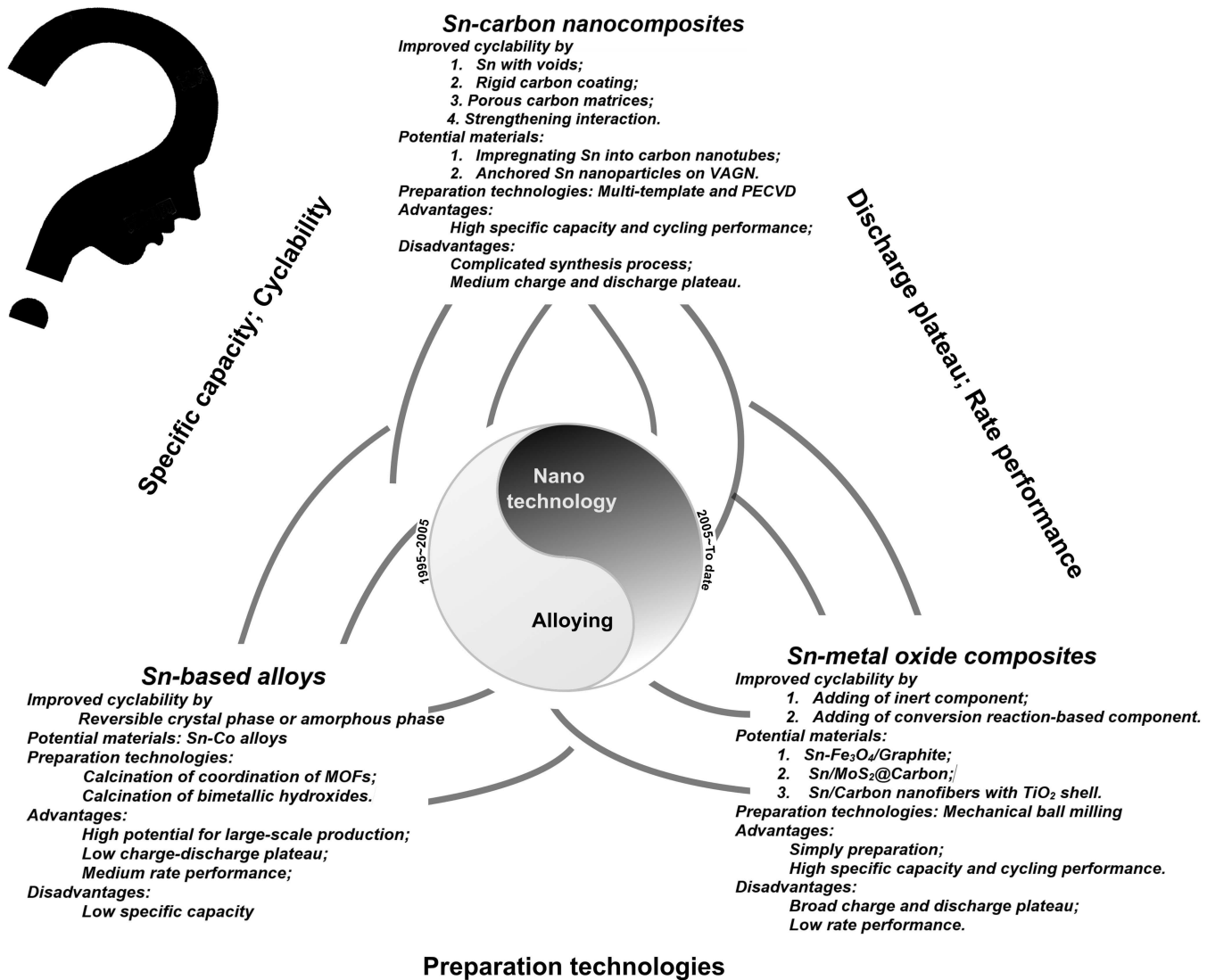


Alloying and Nanotechnology for Sn-based Anode Materials: Paving the Way to the Future of Lithium-Ion Batteries

Shukai Ding,*^[a] Le Zhang,^[a, b] Qingmei Su,*^[a] and Gaohui Du*^[a]



The development of lithium-ion batteries (LIBs) with high energy density is of utmost importance to meet the growing demand for 3 C devices and electric automobiles worldwide. Over the past three decades, there has been significant interest in Sn-based anode materials for LIBs, owing to their high specific capacity and low charge/discharge plateau. Two primary strategies, namely alloying and nanotechnology, have been extensively investigated to enhance the electrochemical performance of Sn-based anodes. However, the complete understanding and recognition of the full potential of these strategies, both in the past and future, remains incomplete. This review aims to provide a comprehensive discussion on the

development of Sn-based anodes prepared using the aforementioned strategies. Furthermore, it emphasizes the practical potential of Sn-based anodes and the associated preparation technologies for large-scale production. Establishing a strong connection between these technologies and high-performance Sn-based composites is crucial, and this objective will be achieved through an extensive comparison and detailed introduction of relevant concepts. By addressing these aspects, this review will contribute to the advancement of Sn-based anodes research and its application in high-performance LIBs, ultimately driving progress in the field of energy storage.

1. Introduction

The increasing demand for batteries with high energy density is obvious in today's world dominated by artificial intelligence due to the proliferation of robots, smartphones, electric automobiles, drones, and wearable devices.^[1,2] To address this urgent need, it is crucial that the development of anode materials that offer cost-effectiveness, safety, and high electrochemical performance.^[3–10]

Over the past 25 years, numerous anode materials have been proposed based on different lithium storage mechanisms. These include graphite-based materials utilizing intercalation reactions, Sn/Si-based materials employing alloying-dealloying reactions, and metal oxide-based materials relying on conversion reactions.^[11–15] The ideal anode materials should possess high energy density, excellent cyclability, low discharge potential, and cost-effectiveness. Among these materials, Sn-based anodes have garnered significant attention due to their abundance in the Earth's crust, high lithium storage efficiency achieved through alloying reactions ($\text{Li}_{4.4}\text{Sn}$ offering a capacity of 993 mAh g^{-1}), and low potential (< 0.5 V versus Li/Li^+).^[16–20] However, the commercialization of Sn-based anodes still faces a major challenge in the poor cyclability caused by significant electrode pulverization resulting from the substantial volume changes (~300%) during cycling.^[21,22]

Sn-based anodes have been extensively examined in previous studies.^[2,17,23–27] However, there has not been a comprehensive review addressing the impact and limitations of preparation strategies, particularly in terms of alloying and nanotechnology. From 1995 to 2005, research primarily focused on the Sn-based alloy anode for obtaining a reversible phase during cycling. Since 2005, significant attention has been drawn

to simple binary Sn-carbon anodes due to the lightness and high conductivity of carbon, and the mechanical buffer effect resulting from the special morphology achieved by the nanotechnology. Notably, the morphology of Sn-carbon anodes has a substantial influence on their electrochemical performance. For instance, by uniformly dispersing Sn nanoparticles within a porous carbon matrix, an ultra-high performance can be achieved. However, the preparation process of Sn-based alloys is simpler and more scalable. Therefore, this review aims to highlight Sn-based anodes exhibiting comparable performance and prepared through alloying and nanotechnology strategies. These preparation technologies in two strategies will be assessed from a practical and scalable standpoint. It is important to mention that studies involving $\text{Sn}-\text{O}$,^[28] $\text{Sn}-\text{S}$,^[29,30] and $\text{Sn}-\text{Se}$ ^[31] based anodes have been excluded from this review due to their inherent deficiency of high irreversible capacity in the initial cycle.

2. Sn-based Alloys Anode

In 1997, Fujifilm Corporation introduced an amorphous $\text{Sn}-\text{M}-\text{O}$ ($\text{M}=\text{B}, \text{P}$, and Al) anode with a high specific capacity. However, its commercialization was unsuccessful due to poor cyclability.^[32] It can be attributed to the significant volume change during the lithiation and delithiation processes, leading to the continuous formation of new interfaces between the electrode and electrolyte. Furthermore, it leads to rapid capacity fading and electrode detachment from the collector. Therefore, the main focus was placed on mitigating the volume change of the electrode during cycling.^[33–35]

2.1. Sn_xM_y alloys: Incorporating inactive elements (Fe, Cu, Ni, and Co)

The Sn_xM_y alloys, where M can be either active or inactive with Li, have been found to possess the capability to form a reversible crystal phase, effectively mitigating volume expansion. Furthermore, the M elements serve as mediators for electron and Li^+ ion transfer. During the initial stages, many metallic elements were chosen for the preparation of Sn-based alloys. For example, L.Y. Beaulieu and J. R. Dahn presented the

[a] Prof. S. Ding, L. Zhang, Prof. Q. Su, Prof. G. Du
Materials Institute of Atomic and Molecular Science
Shaanxi University of Science and Technology
Xi'an 710021 (China)
E-mail: dingshukai@sust.edu.cn
qingmeisu@sust.edu.cn
dugaohui@sust.edu.cn

[b] L. Zhang
School of Materials Science & Engineering
Shaanxi University of Science and Technology
Xi'an 710021 (China)

Sn–Mn alloy anode in LIBs.^[36,37] Besides, Takao Esaka and his colleagues tried the CeSn₃ alloy anode. However, it was fast awarded that these alloys have the poor electrochemical performance.^[38] Thus, the main task of Sn-based anode was focused on the Fe, Cu, Ni, and Co. Sn_xM_y alloys (M=Fe, Cu, Ni, Co) are easily prepared by the mechanical ball milling of a mixture of metal powders, although these alloys' specific capacity was generally less than 300 mAh g⁻¹.^[39–53] It was attributed to heterogeneous particle size and uncontrollable crystal phases in Figure 1(a).

A series of technologies such as solvothermal and nano-precipitation technology, were introduced to prepare nano Sn–Fe alloy. For example, J.P. Tu synthesized monodisperse Sn₂Fe nanospheres (80 nm) and heterogeneously dispersed irregular Sn₂Fe nanoalloys (30–70 nm) using solvothermal and reductive precipitation reactions, respectively.^[54] Wei-Qiang Han prepared Fe_{0.74}Sn₅ nanoalloys (45 nm) by a polyol wet-chemistry reaction.^[39,40] The typical morphology of Sn–Fe nanoalloys was shown in Figure 1(b). M. Stanley Whittingham employed a mechanochemical synthesis to produce Sn₂Fe–carbon composites, where Ti was used as the reduction agent to reduce SnO in the presence of carbon.^[55] As a result, the phase transformation from Sn₂Fe's crystalline phase to amorphous phase can improve the cyclability of the Sn–Fe alloy anode.^[55,56] Hongxia Shi and colleagues introduced the Sn–Fe@C network using the sol-gel method.^[57] Ping Wu reported a 3D Sn–Fe nanoalloys (2.7 nm)/carbon matrix porous network prepared by calcination of double network aerogel in Figure 1(c).^[58] Finally, it increased to a specific capacity of 516 mAh g⁻¹ after 500 cycles in Table 1. Consequently, the Sn₂Fe alloy as anode has a higher specific theoretical capacity and cyclability than other Sn–Fe

alloys due to its tetragonal structure and reversible crystal phase ($\text{Sn}_2\text{Fe} + 8.8 \text{ Li} \rightleftharpoons 2\text{Li}_{4.4}\text{Sn} + \text{Fe}$). The tetragonal structure provided channels between Sn atoms for the penetration of lithium ions.

Sn–Cu alloy has garnered more attention due to in-situ formation by a Cu foil current collector reaction with Sn. Unlike the Sn–Fe alloy, the electrochemical performance of the Sn–Cu alloy demonstrated the dependence on the adhesion force with the Cu collector. In detail, H.-J. Sohn, Noriyuki Tamura, Xiangming He, and Meilin Liu et al. used different technologies, such as chemical reduction reaction and electrodeposition to prepare Sn–Cu anode, but the poor performance was less than 300 mAh g⁻¹.^[59–63] Even, Shi-Gang Sun obtained a three-dimensional macroporous Sn–Cu alloy by a soft polystyrene nanoparticle template during electrochemical deposition (PS-ED), and the reversible capacity was still suspended at 350 mAh g⁻¹ after 70 cycles.^[64] Moreover, the PS-ED technology also was applied to obtain Sn–Ni, Co, and SnSb-based quaternary alloy, although the electrochemical performance hasn't presented an advantage compared to the Sn-based alloy prepared by other technologies in Table 1.^[65–69]

To improve the adhesion force, Aishui Yu utilized Cu foam to deposit Sn by electroless plating. Finally, the improved performance (a specific capacity of 400 mAh g⁻¹ at 100 cycles) proved that the strong adhesion force with the Cu collector is beneficial for cyclability in Table 1.^[70] Thus, J.-M. Tarascon developed a Sn–Cu₆Sn₅ layer on Cu nano-pillar collectors using pulsed electrodeposition technology with an alumina oxide membrane template (PET/AAO) as shown in Figure 1(d), which has an ultra-high areal capacity of 0.02 mAh cm⁻². J.-M. Tarascon claimed that pulsed electrodeposition technology is simple and



Shukai Ding currently holds the position of associate Professor at Shaanxi University of Science and Technology. In 2016, he earned his Ph.D. from Institut Charles Sadron, Université de Strasbourg. His research revolves around comprehending and advancing diverse nanomaterials with applications ranging from high-energy batteries to drug carriers and contrast agents.



Le Zhang received her bachelor's degree in School of Physics and Optoelectronic Technology, Baoji University of Arts and Sciences in 2020. She is currently pursuing her master's degree under the supervision of A/Prof. Shukai Ding in Shaanxi University of Science and Technology. Her research focuses on lithium and potassium-ion batteries.



Qingmei Su is a Professor at Shaanxi University of Science and Technology. She received her Ph.D. degree in Materials Science and Engineering from Taiyuan University of Technology in 2014. Her research interests mainly involve structure characterization of functional materials at atomic scale using an aberration-corrected scanning transmission electron microscopy (STEM), the structure optimization and mechanism exploration of electrode materials for high-energy batteries, including Li-ion batteries, Li metal, solid-state batteries, and Li-S batteries through in-situ STEM and other advanced techniques.



Gaozhi Du is currently a Professor at Shaanxi University of Science and Technology. He received his Ph.D. degree in Condensed Matter Physics from Institute of Physics, Chinese Academy of Sciences in 2003. He has been a researcher at University of Antwerp, Arizona State University, Florida International University, and Zhejiang Normal University. His research interests focus on the understanding and development of various nanomaterials for high-energy batteries, including lithium-ion, sodium-ion, potassium-ion, lithium-sulfur batteries.

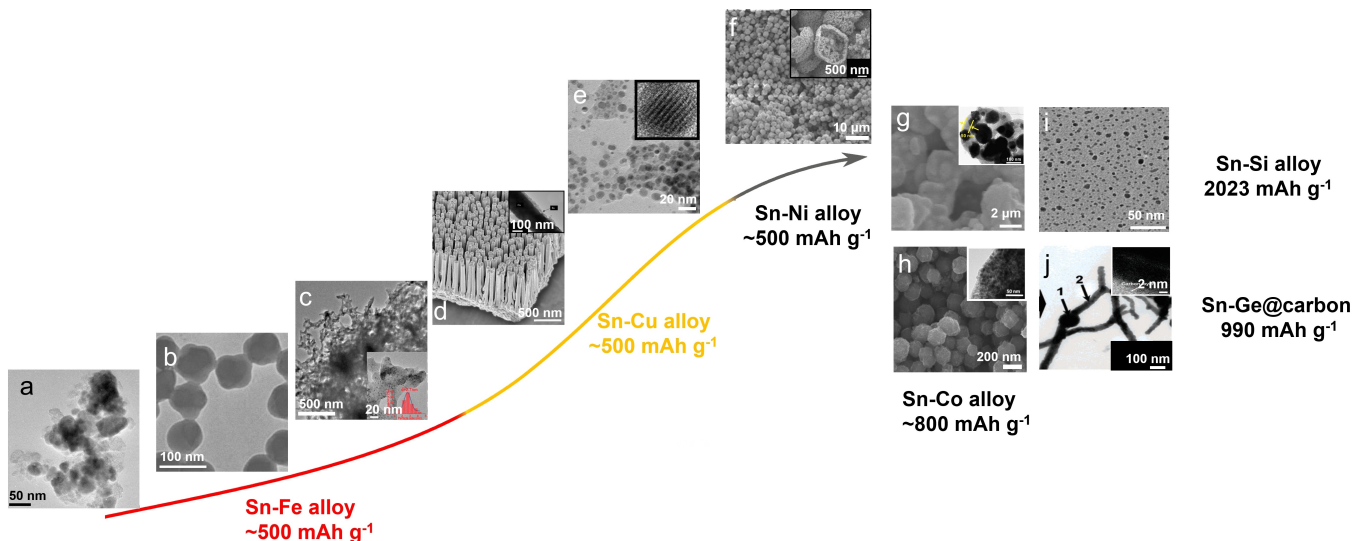


Figure 1. Morphology of Sn–Fe alloy anode prepared a) by mechanical ball milling (Reproduced from Ref. [172] Copyright (2008) with permission from Elsevier), b) by solvothermal and reductive precipitation reactions (Reproduced from Ref. [54] Copyright (2007) with permission from Elsevier), and c) by calcination of double network aerogel. Reproduced from Ref. [58] Copyright (2018) with permission from American Chemical Society. Morphology of Sn–Cu alloy anode prepared d) by the pulsed electrodeposition technology (Reproduced from Ref. [71] Copyright (2008) with permission from Elsevier), and e) by a partial redox transmetalation reaction. Reproduced from Ref. [73] Copyright (2010) with permission from Wiley-VCH. f) Morphology of Sn–Ni alloy anode prepared by the template-free Ostwald ripening-based solvothermal route. Reproduced from Ref. [82] Copyright (2014) with permission from American Chemical Society. Morphology of Sn–Co alloy–Carbon anode prepared g) by calcination of coated $\text{SnCo}(\text{OH})_6$ by dopamine hydrochloride (Reproduced from Ref. [100] Copyright (2018) with permission from American Chemical Society), and h) by calcinating the coordination of Sn salt and ZIF-67. Reproduced from Ref. [99] Copyright (2017) with permission from Royal Society of Chemistry. i) Morphology of Sn–Si alloy prepared by vacuum calcination of butyl-capped analogs. Reproduced from Ref. [105] Copyright (2008) with permission from Royal Society of Chemistry. j) Morphology of Sn–Ge@carbon by superbase butyllithium as a carbon source and a reduction agent for metal salt. Reproduced from Ref. [34] Copyright (2007) with permission from American Chemical Society.

low-cost. However, the mass weight of Sn in one coin cell was only 1.968×10^{-5} g, which was significantly lower than the usual mass weight of 1×10^{-3} g for the active substance.^[71,72] In addition, Jaephil Cho employed a partial redox transmetalation reaction to synthesize Sn(core)-Cu(shell) nanoparticles (Figure 1e), which has the specific capacity of 570 mAh g^{-1} after 170 cycles in a full cell in Table 1.^[73] Qichun Zhang formed the Cu–Sn–S (CTS) Framework using the surfactant-thermal method.^[74,75]

Both Bruno Scrosati and Tetsuya Osaka separately prepared Sn–Ni alloy films by electrodeposition.^[76,77] As a result, small Sn–Ni grains with low crystallinity (shown in the XRD pattern) resulted in a specific capacity of over 650 mAh g^{-1} around the 70th cycle for the first time. A reversible reaction during the charge/discharge process can be attributed to the Ni_3Sn_4 alloy and expressed as follows: First cycle: $\text{Ni}_3\text{Sn}_4 + 17.6\text{Li}^+ + 17.6\text{e}^- \rightleftharpoons 4\text{Li}_{4.4}\text{Sn} + 3\text{Ni}$. Following cycles: $\text{Sn} + 4\text{Li}^+ \rightleftharpoons \text{Li}_{4.4}\text{Sn}$.^[76,78] It seemed that the Sn–Ni alloy electrode underwent an irreversible reaction during the first cycle, which resulted in the formation of Ni and $\text{Li}_{4.4}\text{Sn}$. This irreversible reaction made the Sn–Ni alloy more prone to aggregate compared to Sn₂Fe, which accelerated the peeling off from the Cu collector. Sequentially, Bruno Scrosati coated Ni_3Sn_4 nanoparticles@Cu nanorods onto a Cu plate collector by the PET/AAO technology. Surprisingly, the electrode showed a reversible capacity of 500 mAh g^{-1} after 200 cycles.^[79] Chan-Hwa Chung reported a highly porous dendritic Sn–Ni foam with the predominant phase of Ni_3Sn_4 prepared by the electrodeposition

accompanying the hydrogen evolution reaction.^[80] Yawen Tang and his colleagues immobilized a porous network of Sn–Ni alloy within carbon/graphene dual matrices by the sol-gel method (mixing of dispersed graphene oxide nanosheets SnCl_4 solution and $\text{K}_2\text{Ni}(\text{CN})_4$ solution).^[81] The porous Sn–Ni alloy prepared by the above-discussed three strategies showed the same electrochemical performance in Table 1. The specific capacity was limited to around 500 mAh g^{-1} less than 100 cycles. Yan Yu and his colleagues proposed porous intermetallic micrcages self-assembled by Sn–Ni nanoparticles in Figure 1(f) synthesized by the template-free Ostwald ripening-based solvothermal route, which showed an excellent stable capability (530 mAh g^{-1} after 1000 cycles) in Table 1.^[82,83] The performance was attributed to the nanosized hollow core's structure.

On the other side, Ling Hu and his colleagues also investigated the Sn–Ni alloy electrodes on a Cu foam collector. The resulting reversible capacity of 501 mAh g^{-1} at the 50th cycle.^[84] Hyuk-Sang Kwon investigated the morphological effect of the Cu collectors with the smooth-type morphology and nodule-type morphology.^[85] The Sn–Ni alloy on the Cu collector with the nodule-type morphology demonstrated a higher capacity than the one from the smooth-type morphology. The Sn–Ni alloy on the Cu collector with the nodule-type morphology showed an amorphous state, which exhibited an enhanced specific capacity of 650 mAh g^{-1} for up to 24 cycles. This was attributed to the improved adhesion force between the active material and substrate.

Table 1. Electrochemical performance of Sn-based alloys.

Materials	Specific capacity [mAh g ⁻¹]	Cycling number	Preparation process	Reference
Sn–Fe anode	750	15	Polyol wet chemistry	[39,40]
	500	20	Solvothermal/ precipitation	[54]
	450	270	Mechanochemistry	[55]
	441.6	100	Sol-gel method	[57]
	516	500	Calcination of double network aerogel	[58]
Sn–Cu anode	0.02 mAh cm ⁻²	500	PET/AAO	[71]
	570 in full cell (Li ₂ Co ₃ as cathode)	170	Partial redox transmetalation	[73]
	350	70	PS-ED	[64]
	404	100	Electroless plating	[70]
	536	100	Surfactant-thermal method	[74,75]
Sn–Ni anode	530	1000	Template-free Ostwald ripening-based solvothermal	[82]
	556	75	PS-ED	[65]
	650	70	Electrodeposition	[77]
	500	200	Electrodeposition	[79]
	530 at 1 C	50	Electrodeposition with hydrogen evolution reaction	[80]
Sn–Co anode	818	100	Calcining the coordination of Sn salt and ZIF-67	[99]
	807	180	Calcination of SnCo(OH) ₆ coated with dopamine hydrochloride	[100]
	600	75	PS-ED	[68]
	769	40	Electrodeposition	[87,88]
	563.5	90	Electrodeposition	[89,90]
	700	30	Magnetron sputtering	[95,96]
Sn–Ge alloy	560	80	Electrospinning	[98]
	990	45	Calcination of superbase butyllithium as a carbon source and a reduction agent for metal salt	[34]
Sn–Si alloy	2032	60	Vacuum calcination of butyl-capped analogs	[105]
Fe–Sn–Sb–P alloy	627	80	Electrodepositing	[69]
Sn–Zn alloy	797 mAh cm ⁻³	100	Plastic deformation	[101]

Noriyuki Tamura at Sanyo Electric Company showed the Sn (92.1 wt.%)–Co (7.9 wt.%) alloy film having 769 mAh g⁻¹ up to the 40th cycle. The performance was owed to the amorphous phase at high Sn content and the micro-island structure.^[86–88] Shichao Zhang showed the electrodeposited Sn–Co alloy on a Cu collector with Ni nanocone (200 nm) array. XRD and EDX analysis showed that the multi-crystal phase of Co₃Sn₂, CoSn, CoSn₂, and α-CoSn₃ at a weight ratio of Sn (66.4): Co (33.6), which achieved at 563.5 mAh g⁻¹ at the 90th cycle.^[89,90] Thus, Sn–Co alloy presented higher potential than the other alloys as the anode in LIBs due to high specific capacity.

To further improve performance of Sn–Co alloy, Sn–Co–carbon ternary composites have garnered significant attention due to their use in commercial hybrid LIBs (Nexelion) developed by Sony in 2005.^[91] J.R. Dahn developed a high-throughput magnetron sputtering method (CHMS) to investigate the Sn_{1-x}M_x (M=Ti, V, Cr, Mn, Fe, Co, Ni, Cu) films. As a result, Sn_{1-x}M_x films at the amorphous phase, i.e., Sn–Ti, V, Cr, and Co alloy

presented higher capacity retention with cycles compared to Sn–Mn, Fe, Ni, and Cu alloys. In the case of the Sn–Co anode, the amorphous range can be reached at only $x=0.28$, which resulted in the largest initial specific capacity. However, the cyclability of the Sn–Co alloy was worse than the one of the Sn–V alloy and the Sn–Ti alloy.^[92–94] Furthermore, a systematic investigation of Sn–M (M=V, Co, and Ti)-carbon ternary composites was conducted.^[95] It was found that the addition of carbon in Sn–Co alloy can maintain an amorphous phase during cycling. Conversely, the addition of carbon in Sn–Ti and Sn–V alloys led to the precipitation and crystallization of Sn due to the formation of Ti-carbides and V-carbides. Thus, two Sn_{0.42}Co_{0.34}C_{0.24} and (Sn_{0.55}Co_{0.41-y}C_y) at $y=0.4$ films showed a specific capacity of around 600 mAh g⁻¹ and 700 mAh g⁻¹ after 30 cycles in Table 1.^[95,96] To reduce the content of the noble metal Co, transition metals such as Ti, V, Cr, Mn, Fe, Ni, and Cu have been incorporated to form the quaternary system of Sn–Co–TM–C. Similar electrochemical performance as Sn–Co–C

composites was obtained.^[97] Thus, Sn–Co alloy presented high potential as an anode material of LIBs.

Wan-Jin Lee utilized electrospinning technology to embed Sn–Co nanoalloys (32 nm, 67.2 wt.%) in carbon nanofibers (CNF).^[98] This resulted in a reversible capacity of 560 mAh g⁻¹ over 80 cycles in Table 1. Huaihe Song embedded Sn–Co nanoalloys in porous N-doped carbon microboxes (Figure 1h) by calcining the coordination of Sn salt and ZIF-67, which achieved excellent performance with a specific capacity of 818 mAh g⁻¹ after 100 cycles in Table 1.^[99] Similarly, Jingjing Tang encapsulated Sn–Co nanoalloys in N-doped carbon hollow cubes by calcination of SnCo(OH)₆ coated with dopamine hydrochloride in Figure 1(g).^[100] This approach achieved a reversible capacity of 807 mAh g⁻¹ even after 180 cycles. Interestingly, Arumugam Manthiram utilized severe plastic deformation to prepare Zn–Sn interdigitated eutectic alloy (IdEA) foils, which was considered a scale-up technology. The Zn–Sn alloy was converted into a nanostructured composite of Sn domains distributed in a zinc matrix. The resulting composite exhibited a volumetric capacity of 797 mAh cm⁻³ after 100 cycles.^[101]

2.2. Sn_xM_y alloys: Incorporating active elements (Si, Ge, and Sb)

Incorporating inactive elements with Sn sacrificed the theoretical capacity. The addition of active elements such as Si, Sb, and Ge to synthesize the Sn-based alloys has attracted significant interest.

J. R. Dahn studied SiSn alloy film anode prepared by magnetron sputtering and found that Si₈₅Sn₁₅ and Si₆₃Sn₃₇ were amorphous when the Sn content was less than 58 atom%. Additionally, the starting crystal state remained during the whole lithiation and delithiation process. For example, there was no aggregation of Sn in the Si₆₃Sn₃₇ film electrode during cycling due to the initial amorphous phase.^[102] Thus, Si_{1-x}Sn_x (0 < x < 0.5) has a high potential for improving stability. The addition of misch metals (MM) such as La, Ce, Pr, Nd, Fe, and Mg to the SiSn alloy was beneficial for the formation of an amorphous phase. Over 200 types of Si_{1-x-y}Sn_xMM_y alloys were studied. However, it resulted in the decrease of initial capacity from 2000 to 1000 mAh g⁻¹ and a reversible capacity presented in less than 30 cycles.^[103,104] Surprisingly, Jaephil Cho synthesized carbon-coated Si₇₀Sn₃₀ nanoalloys by vacuum calcination of butyl-capped analogs (Figure 1i).^[105] A high specific capacity of 2032 mAh g⁻¹ after 60 cycles in Table 1.

The Sn₇₈Ge₂₂@carbon Core–Shell nanowires were also constructed by superbase butyllithium as a carbon source and a reduction agent for metal salt (Figure 1j). These nanowires showed a high specific capacity at 990 mAh g⁻¹ after 45 cycles and an 80% retention capacity at a current density of 6400 mA g⁻¹ in Table 1.^[34]

Xuejie Huang prepared SnSb nanoparticles (40–150 nm) by co-reduction of the SnCl₃ and SbCl₃ solution with powder Zn. Then, the SnSb nanoparticles were embedded into carbon microparticles, although the studded alloy nanoparticles did

not have an advantage over pure carbon microparticles.^[106] Martin Winter prepared Sn/SnSb powder (15 nm) using a chemical precipitation reaction. This powder exhibited a specific capacity of 500 mAh g⁻¹ over 50 cycles.^[107] The reaction during charge/discharge cycles was believed to proceed as follows: SnSb + 7.4 Li + 3e⁻ ⇌ Li₃Sb + Li_{4.4}Sn. An attempt was made to reduce the size of Sn–Sb alloy by slowly adding the precursor solution dropwise to the NaBH₄ solution. The specific capacity of the powder decreased slowly from the initial 800 mAh g⁻¹ to 200 mAh g⁻¹ after 30 cycles.^[108] P. Nithyadharseni et al. prepared a ternary system Sn–Sb–M (M=Fe, Co, and Ni) using the reductive co-precipitation method.^[109] The Sn–Sb–M alloys had a smaller size and lower crystallization than pure Sn–Sb alloy. These ternary composites resulted in a high initial capacity (Sn–Sb–Fe, 1680 mAh g⁻¹; Sn–Sb–Co, 2630 mAh g⁻¹; and Sn–Sb–Ni, 1565 mAh g⁻¹). However, the gradual fading resulted in the specific capacity of Sn–Sb–Fe (530 mAh g⁻¹), Sn–Sb–Co (580 mAh g⁻¹), and Sn–Sb–Ni (470 mAh g⁻¹) at the 50th cycle.^[110]

3. Sn–Metal Oxide Composites Anode

As discussed above, mechanical ball milling is the simplest and most scaled-up process, although there is not any advantage of electrochemical performance so far. Seok-Gwang Doo and Hun-Joon Sohn proposed adding materials with high Mohs hardness, such as Al₂O₃, to prepare Sn–Fe alloy during mechanical ball milling. As a result, the addition of 3 wt.% Al₂O₃ led to a capacity of 477 mAh g⁻¹ (73% of the initial charge capacity) after 40 cycles.^[111] Then, Cu powder (10 wt.%) was added instead of Al₂O₃. The composites exhibited a more stable capacity of approximately 470 mAh g⁻¹ over 100 cycles and coulombic efficiency due to the formation of nanosized amorphous Sn₂Fe and Cu₆Sn₅ crystallites during cycling.^[112] Jusef Hassoun hybridized Sn, Fe₂O₃, and carbon by mechanical ball milling. During cycling, the Sn, Fe₂O₃, and carbon separately followed the alloying–dealloying reaction, conversion reaction, and intercalation reaction for the lithium storage. The composites (the weight ratio of Sn: Fe₂O₃ : carbon = 4:3:3, the theoretical capacity of 810 mAh g⁻¹) showed an approaching theoretical specific capacity of 820 mAh g⁻¹ after 100 cycles at 1 C.^[113] Renzong Hu and his colleagues utilized the P-milling technology to create a composite of Fe₃O₄, Sn, and graphite in Figure 2(a),^[114] which delivered a discharge capacity of 793 mAh g⁻¹ in the 240th cycle at 200 mA g⁻¹ and 750 mAh g⁻¹ in the 500th cycle at a current density of 2000 mA g⁻¹ (Table 2).^[115] Furthermore, Ying Wang synthesized Sn nanoparticles well-dispersed in the microspheres of Mn_{0.54}Ni_{0.13}Co_{0.13}(CO₃)_{0.8} (Sn@MNCCO₃) using a one-step solvothermal process. The composites delivered a specific capacity of 560 mAh g⁻¹ after 100 cycles.^[116] Chunsheng Wang covered Sn/carbon nanofibers with a rigid shell of TiO₂ through electrospinning and atomic layer deposition (ALD) (Figure 2b). The resulting electrode delivered a discharge capacity of 831 mAh g⁻¹ after 200 cycles (Table 2).^[117] Yong Wang presented yolk-shelled Sn–MnO@nitrogen-doped carbon composites with three-dimensional interconnected networks (Figure 2c) by calci-

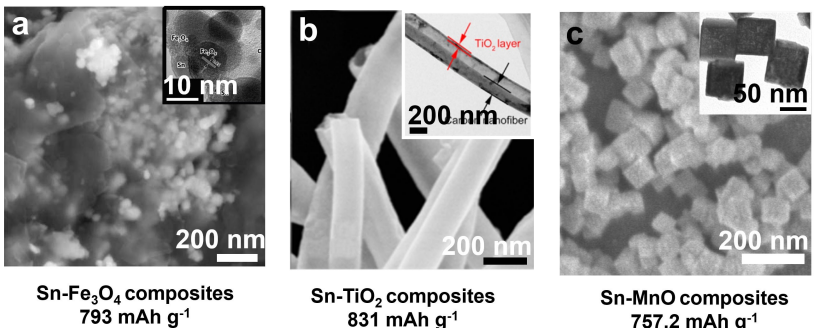


Figure 2. Morphology of Sn-metal oxide composites prepared a) by the P-milling technology (Reproduced from Ref. [115] Copyright (2016) with permission from Royal Society of Chemistry), b) by electrospinning and atomic layer deposition technology (Reproduced from Ref. [117] Copyright (2017) with permission from American Chemical Society), and c) by calcination of dopamine hydrochloride coating MnSn(OH)_6 nanocubes. Reproduced from Ref. [118] Copyright (2018) with permission from Elsevier.

Table 2. Electrochemical performance of Sn-metal oxide composites.

Materials	Specific capacity [mAh g^{-1}]	Cycling number	Preparation process	Reference
$\text{Fe}_3\text{O}_4/\text{Sn}/\text{graphite}$	$750 \text{ at } 2 \text{ A g}^{-1}$	500	P-milling technology	[115]
$\text{Sn/MoS}_2@\text{carbon}$	741	150	Multi-hydrothermal-annealing reaction	[122]
Covered Sn/carbon nanofibers with TiO_2 shell	831	200	Electrospinning and ALD	[117]

nation of dopamine hydrochloride coating MnSn(OH)_6 nanocubes. The composite exhibited a reversible capacity of 757.2 mAh g^{-1} at 0.1 A g^{-1} after 200 cycles (Table 2).^[118,119]

Hun-Joon Sohn prepared a 2D Sn_4P_3 anode by the mechanochemical reaction, which resulted in high discharge and charge capacities at the first cycle, 1130 and 900 mAh g^{-1} ($\text{Sn}_4\text{P}_3 + 25\text{Li}^+ + 25\text{e}^- \rightleftharpoons 4\text{Li}_4\text{Sn} + 3\text{Li}_3\text{P}$), respectively. However, acceptable cyclability was achieved only by applying a limit window potential between 0–0.72 V to avoid the intermediate product LiP due to an insulator for Li^+ ions transfer. As a result, the capacity was limited to 370 mAh g^{-1} at the 50th cycle.^[120] Cheol-Min Park reported the SnTe anode by the ball milling, which has high specific capacity (discharge 666.9/charge 591.6 mAh g^{-1}) at first cycle due to the Li storage of Sn and Te at same time. ($\text{SnTe} + 6.25\text{Li}^+ + 6.25\text{e}^- \rightleftharpoons \text{Li}_{4.25}\text{Sn} + \text{Li}_2\text{Te}$). However, the fast fade was observed to 318 mAh g^{-1} at 30th cycle.^[121] Hong-Qiang Wang and colleagues employed a multi-hydrothermal-annealing reaction to composite Sn nanoparticles (100 nm) and the 3D sphere-like structure of $\text{MoS}_2@\text{C}$.^[122,123] The cyclic voltammetry plot demonstrated that both Sn nanoparticles and MoS_2 were involved in the intercalation of lithium. A high reversible capacity of 741.7 mAh g^{-1} after 150 cycles outperformed the $\text{MoS}_2@\text{C}$ composite anode (with a reversible capacity of 525 mAh g^{-1}). Considering the performance and complicated preparation process, 2D materials cannot attract interest for application in the industry.

4. Sn-Carbon Nanocomposites Anode

The Sn-based anodes have undergone a revolution with the advent of nanotechnology. The utilization of nano-sized and nanostructured materials has opened up new possibilities for

improving cyclability and capacity. The preparation of dispersed Sn nanoparticles in amorphous carbon is simple and easily achieved by different technologies.^[124,125] A typical morphology was shown in Figure 3(a).

For instance, G.X. Wang produced Sn nanoparticle-carbon composites using mechanical ball milling,^[126] while Jaephil Cho presented coating amorphous carbon onto Sn particles through a straightforward hydrothermal reaction involving glucose.^[127] Jusef Hassoun encapsulated Sn nanoparticles within a carbon matrix by directly calcinating a mixture of Sn nanoparticles and coal pitch.^[128] Xueliang Sun achieved the encapsulation of Sn within an amorphous carbon nanotube on a stainless-steel substrate through thermal evaporation and pyrolysis processes.^[129] Bruno Scrosati prepared Sn-carbon composites by calcinating tributylphenyltin impregnated into resorcinol (benzene-1,3-diol)-formaldehyde gel.^[124,125] Zhaoxiang Wang successfully dispersed Sn nanoparticles within hard carbon microparticles.^[130] Furthermore, Min Zhu employed P-milling to uniformly disperse Sn nanoparticles within a graphite matrix.^[131]

As a result, amorphous carbon alone lacks sufficient mechanical stiffness to protect Sn nanoparticles from the volume change that occur during cycling. This limitation led to a specific capacity of approximately 450 mAh g^{-1} and poor cycling performance, as shown in Table 3. On the other hand, carbon nanotubes (CNTs) possess adequate stiffness but can only be successfully composite at low Sn content (<40 wt.%) due to the aggregation of Sn nanoparticles at high loading. In a study by Jim Yang Lee, ultra-fine Sn nanoparticles were encapsulated within carbon nanotubes using chemical vapor deposition (CVD) and a porous alumina membrane template, as depicted in Figure 3(b). This approach resulted in a specific capacity of 473 mAh g^{-1} that was maintained after 80 cycles.^[132]

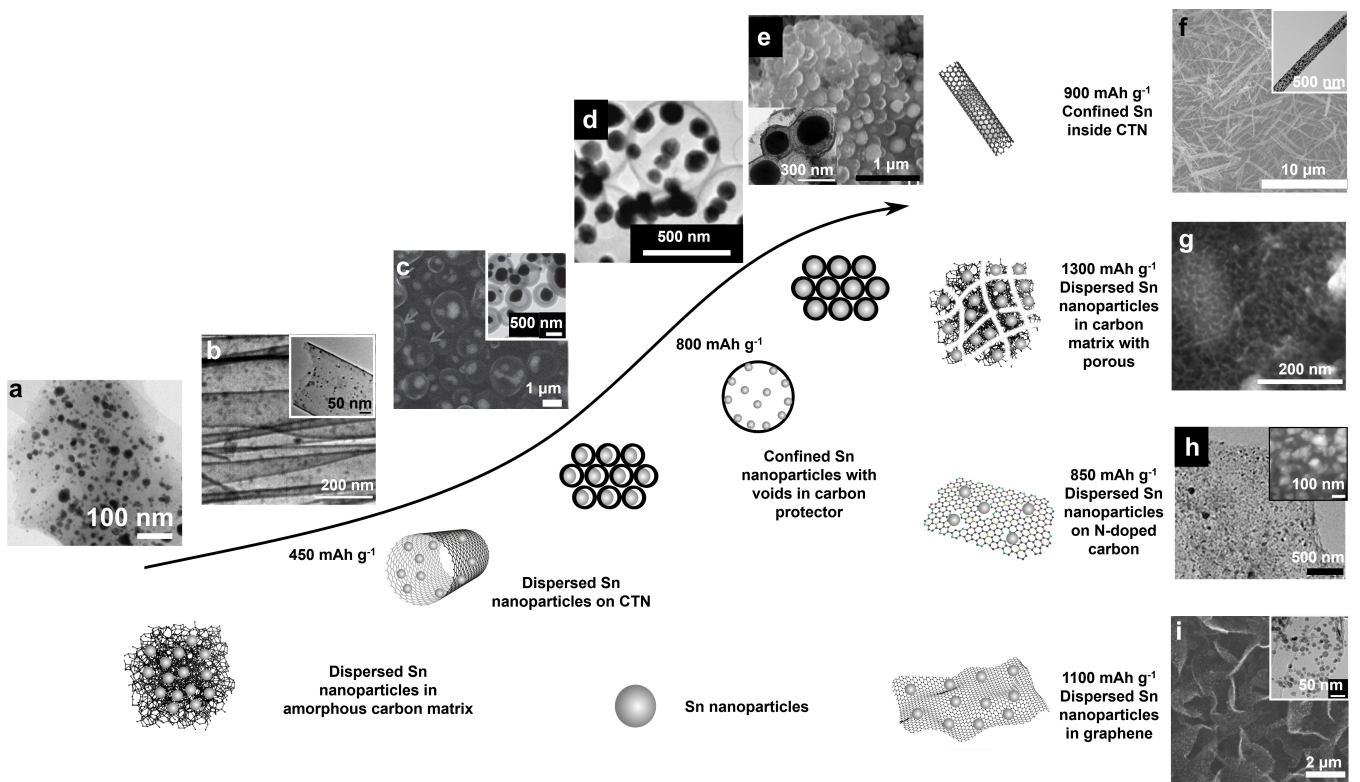


Figure 3. Historic illustration of the development of Sn-carbon anode prepared by nanotechnology. a) Typical morphology of dispersed Sn nanoparticles in an amorphous carbon matrix. Reproduced from Ref. [125] Copyright (2008) with permission from Wiley-VCH. b) Typical morphology of dispersed Sn nanoparticles on carbon nanotube. Reproduced from Ref. [132] Copyright (2009) with permission from American Chemical Society. c-e) Typical morphology of Sn nanoparticles with voids-carbon shell nanoparticles. c) Reproduced from Ref. [133] Copyright (2015) with permission from Wiley-VCH. d) Reproduced from Ref. [134] Copyright (2008) with permission from Wiley-VCH. e) Reproduced from Ref. [138] Copyright (2016) with permission from American Chemical Society. f) Typical morphology of poured Sn inside carbon nanotube. Reproduced from Ref. [16] Copyright (2020) The Author(s). g) Typical morphology of dispersed Sn nanoparticles in carbon matrix with porous. Reproduced from Ref. [149] Copyright (2012) with permission from Royal Society of Chemistry. h) Typical morphology of Sn nanoparticles on N-doped carbon. Reproduced from Ref. [151] Copyright (2020) with permission from American Chemical Society. i) Typical morphology of dispersed Sn nanoparticles on the surface of graphene. Reproduced from Ref. [155] Copyright (2013) with permission from Elsevier.

To improve the electrochemical performance, a typical strategy involves creating voids alongside Sn nanoparticles to accommodate volume changes and applying a rigid carbon coating to resist. Three representative morphologies are depicted in Figure 3(c–e). For instance, Yun Chan Kang obtained Sn nanoparticles with a core-shell structure, where the core consisted of Sn and the shell was composed of carbon, prepared using spray pyrolysis technology with sacrificial Zn nanoparticles.^[133] Li-Jun Wan utilized SiO_2 nanoparticles as templates to achieve an Sn–carbon yolk-shell structure.^[134] Similarly, Shukai Ding dispersed Sn nanoparticles with voids in a graphene matrix using organic nanoframes as precursors in a one-step process.^[135–137] Jun Liu and colleagues self-assembled Sn–void–carbon yolk–shell nanoparticles into a 2D sheet.^[138] Chengzhong Yu created nanoboxes composed of a carbon shell and Sn core using Zn as a sacrificial material and polydopamine as a carbon source.^[139] As a result, the electrochemical performance improved, exhibiting a specific capacity of around 800 mAh g^{-1} over more than 100 cycles, as shown in Table 3.

The CNT intrinsically has voids, high stiffness, and conductivity. Thus, distinct from dispersing Sn nanoparticles in CNT, partially impregnate Sn into CNT (Figure 3f) can offer enough stiffness to resist the volume change. Junhong Chen

poured Sn into the CNT.^[140] Yan Yu and Lin Gu employed coaxial electrospinning technology to impregnate Sn nanoparticles into carbon hollow nanofibers.^[141] David Lou used MnO_x nanowires templates to encapsulate Sn in amorphous carbon nanotubes.^[142] Yufeng Lu and his colleagues developed Sn-graphene tubes by pouring Sn into double-layered graphene tubes. The graphene tube was prepared by CVD using MgO nanowires as the template.^[16] As a result, the structure showed high electrochemical performance (up to 900 mAh g^{-1}) in Table 3.

Simultaneously, the use of a carbon matrix with a porous structure, as illustrated in Figure 3(g), has provided another avenue for mitigating volume changes. Chunlei Wang dispersed Sn nanoparticles within a highly porous carbon matrix using electrostatic spray deposition.^[143] Fengwei Huo employed metal-organic frameworks (MOFs) as a carbon source to construct a three-dimensional structure of Sn–carbon nanocomposites.^[144] Chunsheng Wang achieved the homogeneous dispersion of Sn nanograins within a conductive carbon sphere through aerosol spray pyrolysis under an Ar/H_2 environment.^[145] Similarly, Jun Chen and Lynden A. Archer reported the synthesis of $\text{Sn}@\text{C}$ nanocomposites using aerosol spray pyrolysis.^[146,147] Longwei Yin encapsulated Sn nanopar-

Table 3. Electrochemical performance of Sn-carbon nanocomposites.

Design strategies for Sn-carbon nanocomposites	Specific capacity [mAh g ⁻¹]	Cycling number	Method	Reference
Dispersed Sn nanoparticles in amorphous carbon matrix	400	20	Mechanical ball milling	[126]
	67	30	Hydrothermal reaction with glucose	[127]
	400	100	Calcination mixture of Sn nanoparticles and coal pitch	[128]
	489	330	Thermal evaporation and pyrolyze	[129]
	450	200	Calcination of impregnated tributylphenyltin to resorcinol (benzene-1,3-diol)-formaldehyde (methanol) gel	[124,125]
	400	30	Low-temperature pyrolysis of sugar precursor and Fe(NO ₃) ₃	[130]
Sn nanoparticles with voids and rigid carbon coating	400	40	P-milling	[131]
	691	500	Spray pyrolysis technology and Zn as a sacrificial material	[133]
	550	100	Hydrothermal reaction by Sn salt and urea in water-ethanol solution with SiO ₂ template, etching, then calcination	[134]
	850	50	Hydrothermal reaction by Sn salt and urea in water-ethanol solution	[138]
	539	200	Hydrothermal and calcination of organic nano frames	[135]
	810	500	Polydopamine coating for ZnSnO ₃ and calcination	[139]
Impregnate Sn into carbon nanotube	918	500	CVD using MgO nanowires as the template	[16]
	626	200	CVD and etching by CaCO ₃ -based template	[140]
	737	200	Coaxial electrospinning	[141]
	749	100	Polydopamine coating and CVD by MnO _x nanowires templates	[142]
Dispersed Sn nanoparticles into carbon matrix with porous	1300	300	Calcination by resorcinol-formaldehyde with Pluronic F127	[149]
	638	315	Electrostatic spray deposition	[143]
	740	200	Calcination by MOF	[144]
	700	200	Aerosol spray pyrolysis	[145]
	757	100	Carbon xerogel	[148]
Dispersed Sn nanoparticles on N-doped carbon	854	100	Polydopamine coating and calcination	[151]
	720	200	Calcination of Salen	[150]
Dispersed Sn nanoparticles on graphene	1005	130	MPCVD	[155]
	679	30	Layer-by-layer by exfoliated graphene film and thermal-evaporation Sn films	[152]
	590	60	Hydrothermal reaction of SnO ₂ nanoparticles and GO with glucose	[153]
	1100	30	Microwave-assisted hydrothermal reaction of Sn salt and GO	[154]
	1089	100	CVD with NaCl particles 3D template	[156]

ticles within a carbon xerogel featuring three-dimensional pores.^[148] Furthermore, Chunsheng Wang and his colleagues successfully synthesized sponge-like porous Sn-carbon composites through in-situ carbonization of suspended SnO₂ nanoparticles in a resorcinol-formaldehyde dispersion, using a triblock polymer (Pluronic F127) as a porogen. These composites demonstrated a specific capacity of up to 1300 mAh g⁻¹ after 300 cycles, as indicated in Table 3.^[149]

On the other hand, enhancing the interaction between Sn nanoparticles and the carbon matrix can effectively suppress

the aggregation of Sn nanoparticles during cycling. This interaction can be achieved through heteroatom doping in the carbon matrix, as depicted in Figure 3(h), or by utilizing a graphene substrate with high electron cloud density, as shown in Figure 3(i). The high electron cloud density can be attributed to the presence of lone pair electrons from the heteroatom or π-π conjugation.

For example, Jun Chen embedded Sn nanoparticles within an N-doped porous carbon network by carbonizing a divalent Sn complex, specifically Sn (Salen).^[150] Zaiping Guo reported a

graphene-encapsulated nitrogen-doped carbon@Sn compact monolith using a grade-by-grade coating-growth technique.^[151] Yuegang Zhang directly constructed a freestanding anode by encapsulating Sn nanopillars between graphene layers on copper foils.^[152] Linjie Zhi obtained graphene-confined Sn nanosheets by calcination and reduction of confined SnO₂ nanoparticles between multilayers of graphene oxide (GO).^[153] Guoxiu Wang and Yong Wang dispersed Sn nanoparticles on the surface of graphene using microwave-assisted hydrothermal synthesis (MAHS).^[154] Sn balls were encapsulated by graphene and anchored onto vertically aligned graphene nanosheets (VAGN) through microwave plasma-enhanced chemical vapor deposition (PECVD).^[155] Jian Qin et al. anchored Sn nanoparticles within 3D porous graphene networks (Sn@G-PGNW) using an in-situ chemical vapor deposition (CVD) technique with a 3D template of NaCl particles.^[156] The high specific capacity observed for dispersed Sn nanoparticles on N-doped carbon and graphene was presented in Table 3. It demonstrated the effectiveness of strengthening the interaction between the components on the electrochemical performance of the Sn-based anodes.

Based on the aforementioned discussions, the utilization of voids adjacent to Sn nanoparticles, the construction of a porous carbon matrix, the partial impregnation of Sn into CNT, and the enhancement of the interaction between Sn and carbon have demonstrated the effectiveness of nano-size and nano-structure tuning strategies. These approaches have shown promising results in improving the electrochemical performance of Sn-based anodes.

5. Comprehensive Comparison of Sn-based Anodes: Electrochemical Performance and Preparation Technologies

A wide range of Sn_xM_y alloys, Sn-carbon nanocomposites, and a few Sn-metal oxide composites have been investigated thus far. Among them, 11 types of Sn-based anodes with high potential have been carefully selected based on the specific capacity (exceeding 800 mAh g⁻¹) and cycling performance (over 100 cycles). To further analyze and compare the charge-discharge plateau, rate performance, and the associated preparation technologies, the following anodes were considered: two Sn-Co alloys,^[99,100] Sn-Fe₃O₄/Graphite composites,^[115] Sn/MoS₂@Carbon composites,^[122,123] Sn/carbon nanofibers with TiO₂ shell composites,^[117] Sn nanoparticles with voids and carbon coating composite,^[139] impregnated Sn into carbon nanotube composite,^[16] dispersed Sn nanoparticles into carbon matrix with porous structure,^[149] dispersed Sn nanoparticles on N-doped carbon composite,^[151] and two dispersed Sn nanoparticles on graphene composites.^[155,156]

Attaining a low and stable charge-discharge plateau is of paramount importance for lithium-ion batteries (LIBs) as it ensures consistent and high voltage during operation. Figures 4 and 5 illustrated the cyclic voltammetry (CV) curves and voltage profiles of the aforementioned Sn-based anodes, which have

been divided into three distinct grey regions: 0–0.25 V, 0.25–0.75 V, and 0.75–2 V, as well as 0–200 mAh g⁻¹, 200–400 mAh g⁻¹, and 400–800 mAh g⁻¹, respectively. Figure 4(a and b) revealed that the anodic and cathodic peaks of Sn–Co alloys mainly concentrate below 0.75 V. Notably, Sn–Co alloys prepared by the calcination of SnCo(OH)₆ coated with dopamine hydrochloride exhibited a higher discharge specific capacity of 400 mAh g⁻¹ before reaching 0.75 V (Figure 5a and b) compared to Sn–Co alloys prepared via calcining the coordination of Sn salt and ZIF-67. This indicated the practical value of Sn–Co alloys prepared by calcination of SnCo(OH)₆ coated with dopamine hydrochloride.

The discharge and charge reactions of the Sn-metal oxide anodes, such as Sn-Fe₃O₄-Graphite, Sn-MoS₂-carbon composites, and Sn/carbon nanofibers with TiO₂ shell (Figures 4 and 5c–e), primarily occurred in the range of over 1 V. On the other hand, Sn-carbon nanocomposites (Figure 4f–j) showed an increase in the cathodic peak voltage range from 0.75 V to 1 V compared to Sn–Co alloys. It can be attributed to the electron transfer resistance resulting from the presence of carbon coatings and voids. As a result, Sn-carbon nanocomposites generally offer higher specific capacities than Sn-based alloys but may exhibit lower working voltages in the full cell.

It is worth noting that dispersed Sn nanoparticles in a carbon matrix with porous composites, prepared through the calcination of resorcinol-formaldehyde with Pluronic F127 as a carbon source, demonstrated unstable electrochemical performance.^[149] Examining the rate performance of various Sn-based anodes, Figure 6(a) displayed the Sn–Co alloy prepared by calcining the coordination of Sn salt and ZIF-67, exhibiting a rate performance of approximately 500 mAh g⁻¹ at 2 A g⁻¹, which surpassed that of the Sn–Co alloy prepared through the calcination of SnCo(OH)₆ coated with dopamine hydrochloride (Figure 6b), Sn-Fe₃O₄-Graphite composites (Figure 6c), covered Sn/carbon nanofibers with TiO₂ shell composites (Figure 6d), Sn nanoparticles with voids and carbon coating composites (Figure 6e), dispersed Sn nanoparticles into carbon matrix with porous composites (Figure 6g), and dispersed Sn nanoparticles on N-doped carbon composites (Figure 6h). Among the Sn-carbon nanocomposites, the impregnated Sn into carbon nanotube composites (Figure 6f) and the two dispersed Sn nanoparticles on graphene composites (Figure 6i and j) demonstrated exceptional rate performance. It can be attributed to the high conductivity of graphene.

Overall, these findings highlight the potential of Sn–Co alloys prepared through calcinating the coordination of Sn salt and ZIF-67, as well as the promising rate performance exhibited by Sn-carbon nanocomposites involving carbon nanotubes and graphene structures.

Apart from considering the electrochemical performance, it is crucial to assess the preparation technologies for large-scale production. Understanding the manufacturing processes of the aforementioned Sn-based anodes is essential to pave the way for their commercialization. For instance, the production of Sn–Co alloys through the calcination of Sn salt and ZIF-67 entailed several steps, including chemical reactions, filtration, and drying processes. Metal-organic frameworks (MOFs), which

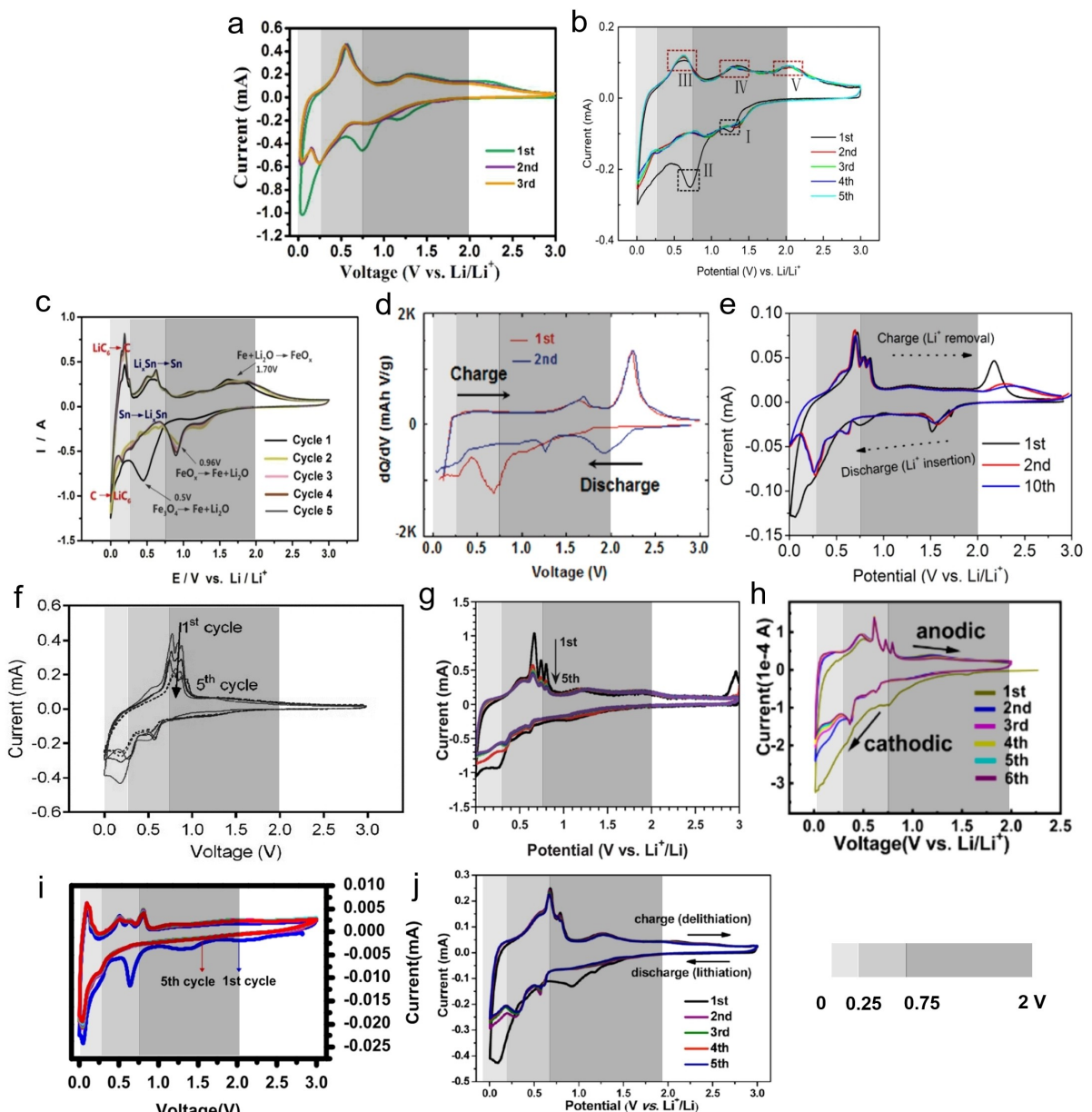


Figure 4. CV curves of Sn–Co alloys prepared by a) calcining the coordination of Sn salt and ZIF-67. Reproduced from Ref. [99] Copyright (2017) with permission from Royal Society of Chemistry. b) Calcination of SnCo(OH)_6 coated with dopamine hydrochloride. Reproduced from Ref. [100] Copyright (2018) with permission from American Chemical Society. c) Sn– Fe_3O_4 -Graphite composites prepared by P-milling technology. Reproduced from Ref. [115] Copyright (2016) with permission from Royal Society of Chemistry. d) Sn– MoS_2 -Carbon composites prepared by multi-hydrothermal-annealing reaction. Reproduced from Ref. [122] Copyright (2011) with permission from American Chemical Society. e) Covered Sn/carbon nanofibers with TiO_2 shell composites prepared by electrospinning and ALD. Reproduced from Ref. [117] Copyright (2017) with permission from American Chemical Society. f) Sn nanoparticles with voids and carbon coating composites prepared by polydopamine coating for ZnSnO_3 and calcination. Reproduced from Ref. [139] Copyright (2017) with permission from Wiley-VCH. g) Dispersed Sn nanoparticles into carbon matrix with porous composites prepared by calcination by resorcinol-formaldehyde with Pluronic F127 as carbon source. Reproduced from Ref. [149] Copyright (2012) with permission from Royal Society of Chemistry. h) Dispersed Sn nanoparticles on N-doped carbon composites prepared by polydopamine coating and calcination. Reproduced from Ref. [151] Copyright (2020) with permission from American Chemical Society. Dispersed Sn nanoparticles on graphene composites prepared by (i) PECVD (Reproduced from Ref. [155] Copyright (2008) with permission from Elsevier), and j) CVD with NaCl particles 3D template. Reproduced from Ref. [156] Copyright (2014) with permission from American Chemical Society.

are porous materials constructed from metal ions and organic ligands, play a significant role in this preparation procedure. Fortunately, MOFs have gained substantial interest across various fields, including catalysis and water treatment.^[157–159] Thus, large-scale production processes and continuous flow chemistry techniques for the preparation of MOFs have been

developed.^[160–164] Furthermore, the transformation of SnCo(OH)_6 into Sn–Co alloy can be achieved by adjusting the pH value of the Co and Sn salt solution.^[165–168] The microfluidic-assisted coprecipitation systems have demonstrated the effective synthesis of SnCo(OH)_6 nanoparticles.

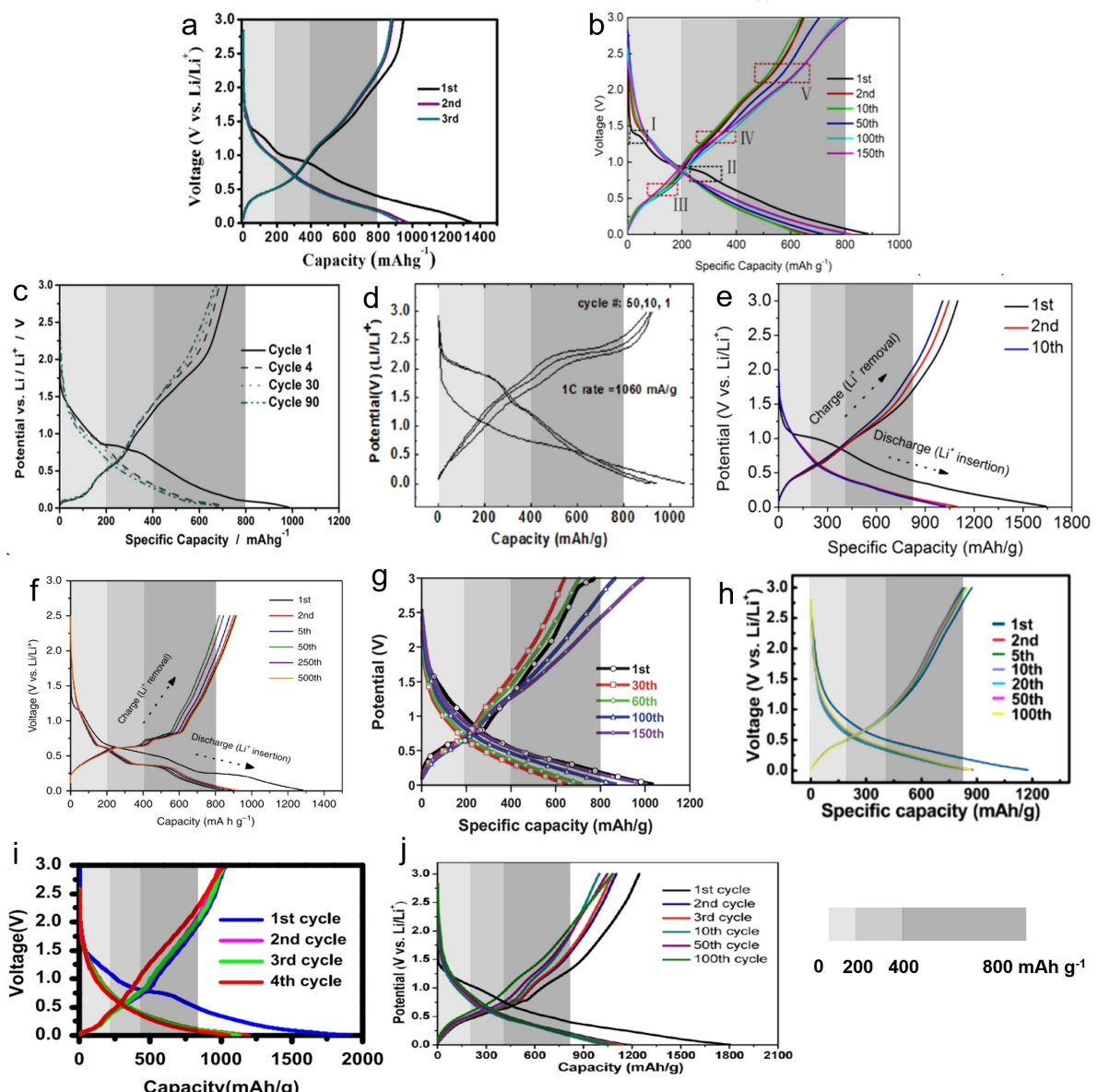


Figure 5. Voltage profiles of Sn–Co alloys prepared by a) calcining the coordination of Sn salt and ZIF-67. Reproduced from Ref. [99] Copyright (2017) with permission from Royal Society of Chemistry. b) calcination of $\text{SnCo}(\text{OH})_6$ coated with dopamine hydrochloride. Reproduced from Ref. [100] Copyright (2018) with permission from American Chemical Society. c) $\text{Sn}-\text{Fe}_3\text{O}_4$ -graphite composites prepared by P-milling technology. Reproduced from Ref. [115] Copyright (2008) with permission from Royal Society of Chemistry. d) $\text{Sn}-\text{MoS}_2$ -Carbon composites prepared by multi-hydrothermal-annealing reaction. Reproduced from Ref. [122] Copyright (2011) with permission from American Chemical Society. e) covered Sn/carbon nanofibers with TiO_2 shell composites prepared by electrospinning and ALD. Reproduced from Ref. [117] Copyright (2017) with permission from American Chemical Society. f) Impregnate Sn into carbon nanotube composites prepared by CVD using MgO nanowires as the template. Reproduced from Ref. [12] Copyright (2020) The Author(s). g) Dispersed Sn nanoparticles into carbon matrix with porous composites prepared by calcination by resorcinol-formaldehyde with Pluronic F127 as carbon source. Reproduced from Ref. [149] Copyright (2012) with permission from Royal Society of Chemistry. h) Dispersed Sn nanoparticles on N-doped carbon composites prepared by polydopamine coating and calcination. Reproduced from Ref. [151] Copyright (2020) with permission from American Chemical Society. Dispersed Sn nanoparticles on graphene composites prepared by i) MPCVD (Reproduced from Ref. [155] Copyright (2013) with permission from Elsevier, and j) CVD with NaCl particles 3D template. Reproduced from Ref. [156] Copyright (2014) with permission from American Chemical Society.

Regarding Sn–carbon composites, impregnating Sn into carbon nanotubes and dispersing Sn nanoparticles onto graphene have shown considerable advantages in terms of electrochemical performance. However, impregnating Sn into carbon nanotubes is a supposed challenge and may not be suitable for scalable production due to the complex modification of the hydrophilic–hydrophobic interface.

On another hand, three-dimensional graphene building materials, including graphene foams and VAGN, have garnered significant attention in the past two decades. The development of PECVD systems has facilitated the growth of VAGN, offering great potential in various fields due to their superior reaction kinetics and mass transportation capabilities.^[169–171] Notably, the preparation process does not require special catalysis on

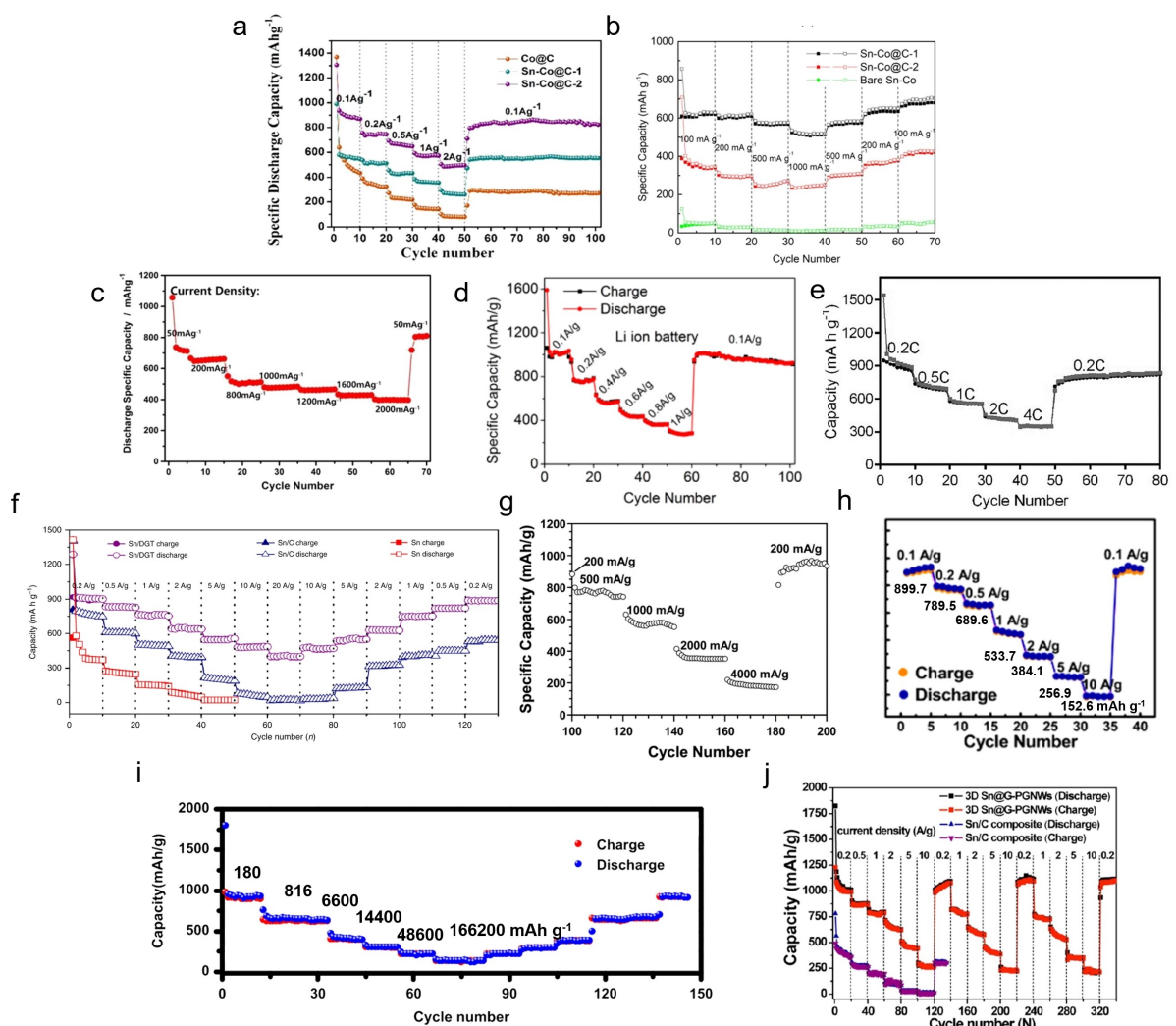


Figure 6. Rate performance of Sn–Co alloys prepared by a) calcining the coordination of Sn salt and ZIF-67. Reproduced from Ref. [99] Copyright (2017) with permission from Royal Society of Chemistry. b) Calcination of $\text{SnCo}(\text{OH})_6$ coated with dopamine hydrochloride. Reproduced from Ref. [100] Copyright (2018) with permission from American Chemical Society. c) $\text{Sn}-\text{Fe}_3\text{O}_4$ -graphite composites prepared by P-milling technology. Reproduced from Ref. [115] Copyright (2016) with permission from Royal Society of Chemistry. d) Sn/carbon nanofibers covered with TiO_2 shell composites prepared by electrospinning and ALD. Reproduced from Ref. [117] Copyright (2017) with permission from American Chemical Society. e) Sn nanoparticles with voids and carbon coating composites prepared by polydopamine coating for ZnSnO_3 and calcination. Reproduced from Ref. [139] Copyright (2017) with permission from Wiley-VCH. f) Impregnate Sn into carbon nanotube composites prepared by CVD using MgO nanowires as the template. Reproduced from Ref. [16] Copyright (2020) The Author(s). g) Dispersed Sn nanoparticles into carbon matrix with porous composites prepared by calcination by resorcinol-formaldehyde with Pluronic F127 as carbon source. Reproduced from Ref. [149] Copyright (2012) with permission from Royal Society of Chemistry. h) Sn nanoparticles dispersed on N-doped carbon composites prepared by polydopamine coating and calcination. Reproduced from Ref. [151] Copyright (2020) with permission from American Chemical Society. Dispersed Sn nanoparticles on graphene composites prepared by i) MPCVD (Reproduced from Ref. [155] Copyright (2013) with permission from Elsevier), and j) CVD with NaCl particles 3D template. Reproduced from Ref. [156] Copyright (2014) with permission from American Chemical Society.

different materials substrates such as quartz and metal. The scalability, controllability, and repeatability of the preparation processes are crucial for future success. Technologies such as mechanochemical synthesis,^[55,120] aerosol spray pyrolysis,^[133,145] P-milling,^[115,131] severe plastic deformation,^[101] and microfluidic-assisted synthesis should be further explored and given more attention due to their potential for scaling up production while ensuring desired material properties.^[168]

In summary, considering the scalability and feasibility of the preparation processes is vital for the successful commercialization of Sn-based anodes. Advances in large-scale MOF production, pH adjustment techniques, and the development of PECVD

systems for 3D graphene materials contribute to the potential practical applications of Sn-based anodes. Additionally, research should focus on optimizing and exploring various preparation methods to achieve scalable, controlled, and repeatable production processes.

6. Conclusions

In summary, the research on Sn-based anodes has undergone extensive exploration, focusing on their preparation using alloying and nanotechnology strategies. Recent studies have

also ventured into more complex systems involving metal oxides, quaternary compounds, and multi-alloy composites. The key findings can be summarized:

1. The specific capacity and cycling performance of Sn-based alloy anodes are primarily influenced by the crystal phase, with reversible crystal and amorphous phases showing the potential for improving cyclability.
2. The specific capacity and cycling performance of Sn-carbon nanocomposites anodes can be improved by introducing the voids, the rigid carbon coating, porous carbon matrices, and the strengthened interaction between carbon and Sn by doping or using graphene.
3. Sn-metal oxide anodes can exhibit high specific capacity and cycling performance by simple mechanical ball milling due to the inertness and rigidity of additional components, as well as the presence of a mixed lithium storage mechanism.

Taking into account factors such as charge/discharge plateau, rate performance, and preparation technologies, it is evident that Sn–Co alloys prepared using MOFs and bimetallic hydroxides offer greater advantages compared to conventional Sn-carbon nanocomposites. These alloy systems exhibit favorable electrochemical performance. On the other hand, the 3D graphene-based Sn-based anode materials demonstrate even higher electrochemical performance, although they may involve greater complexity and higher cost compared to other options.

Acknowledgements

This work was supported by the Foundation of Shaanxi University of Science and Technology (Grant No. 126021823), Key Research and Development Project in Shaanxi Province (2023-YBGY-446), National Natural Science Foundation of China (No. U2032131), and Shanxi-Zheda Institute of Advanced Materials and Chemical Engineering (No. 2022SX-TD012). Thank you to Ms. Rongyu Ding for her contribution in preparing the author's photo. Thank you to the authors and publishers in cited literature for the data permission.

Conflict of Interests

The authors declare no conflict of interest.

Data Availability Statement

The data that support the findings of this study are available from the corresponding author upon reasonable request.

Keywords: Sn-based anode • lithium-ion battery • Sn-based alloy • Sn-based nanocomposites • Nanotechnology

- [1] J. Xie, Y. C. Lu, *Nat. Commun.* **2020**, *11*, 2499.
- [2] M. T. McDowell, S. W. Lee, W. D. Nix, Y. Cui, *Adv. Mater.* **2013**, *25*, 4966.
- [3] Y. Ding, Z. P. Cano, A. Yu, J. Lu, Z. Chen, *Electrochim. Energy Rev.* **2019**, *2*, 1.

- [4] T. Kim, W. Song, D. Y. Son, L. K. Ono, Y. Qi, *J. Mater. Chem. A* **2019**, *7*, 2942.
- [5] C. P. Grey, D. S. Hall, *Nat. Commun.* **2020**, *11*, 2.
- [6] J. B. Goodenough, *Nat. Electron.* **2018**, *1*, 204.
- [7] G. Zubi, R. Dufo-López, M. Carvalho, G. Pasaoglu, *Renewable Sustainable Energy Rev.* **2018**, *89*, 292.
- [8] F. Wu, J. Maier, Y. Yu, *Chem. Soc. Rev.* **2020**, *49*, 1569.
- [9] A. Masias, J. Marcicki, W. A. Paxton, *ACS Energy Lett.* **2021**, *6*, 621.
- [10] G. L. Zhu, C. Z. Zhao, J. Q. Huang, C. He, J. Zhang, S. Chen, L. Xu, H. Yuan, Q. Zhang, *Small* **2019**, *15*, 1.
- [11] K. Feng, M. Li, W. Liu, A. G. Kashkooli, X. Xiao, M. Cai, Z. Chen, *Small* **2018**, *14*, 1702737.
- [12] B. Wang, B. Luo, X. Li, L. Zhi, *Mater. Today* **2012**, *15*, 544.
- [13] M. Zheng, H. Tang, L. Li, Q. Hu, L. Zhang, H. Xue, H. Pang, *Adv. Sci.* **2018**, *5*, 1700592.
- [14] H. Zhang, Y. Yang, D. Ren, L. Wang, X. He, *Energy Storage Mater.* **2021**, *36*, 147.
- [15] S. Liang, Y. J. Cheng, J. Zhu, Y. Xia, P. Müller-Buschbaum, *Small Methods* **2020**, *4*, 2000218.
- [16] R. Mo, X. Tan, F. Li, R. Tao, J. Xu, D. Kong, Z. Wang, B. Xu, X. Wang, C. Wang, J. Li, Y. Peng, Y. Lu, *Nat. Commun.* **2020**, *11*, 1374.
- [17] W. Li, X. Sun, Y. Yu, *Small Methods* **2017**, *1*, 22.
- [18] T. Journal, M. C. Weeks, T. Journal, M. C. Weeks, E. Voss, S. Yoshizawa, S. Okada, R. T. Mathieson, P. Press, E. L. Jones, T. Journal, G. Papazov, D. Pavlov, T. M. Company, E. J. Ritchie, C. Manufacturing, *J. Electrochem. Soc. Sci. Technol.* **1981**, *128*, 725.
- [19] S. R. Taylor, S. M. McLennan, *Chem. Geol.* **1983**, *39*, 273.
- [20] Y. Zhao, X. Li, B. Yan, D. Li, S. Lawes, X. Sun, *J. Power Sources* **2015**, *274*, 869.
- [21] C. K. Chan, H. Peng, G. Liu, K. McIlwrath, X. F. Zhang, R. A. Huggins, Y. Cui, *Nat. Nanotechnol.* **2008**, *3*, 31.
- [22] B. Scrosati, J. Hassoun, Y. K. Sun, *Energy Environ. Sci.* **2011**, *4*, 3287.
- [23] W. J. Zhang, *J. Power Sources* **2011**, *196*, 13.
- [24] A. R. Kamali, D. J. Fray, *Rev. Adv. Mater. Sci.* **2011**, *27*, 14.
- [25] L. Liu, F. Xie, J. Lyu, T. Zhao, T. Li, B. G. Choi, *J. Power Sources* **2016**, *321*, 11.
- [26] H. Ying, W. Q. Han, *Adv. Sci.* **2017**, *4*, 1700298.
- [27] Z. Yi, Z. Wang, Y. Cheng, L. Wang, *Energy Environ. Mater.* **2018**, *1*, 132.
- [28] J. S. Chen, X. W. Lou, *Small* **2013**, *9*, 1877.
- [29] J. Liu, M. Gu, L. Ouyang, H. Wang, L. Yang, M. Zhu, *ACS Appl. Mater. Interfaces* **2016**.
- [30] J. Xia, L. Liu, S. Jamil, J. Xie, H. Yan, Y. Yuan, Y. Zhang, *Energy Storage Mater.* **2019**, *17*, 1.
- [31] Z. X. Huang, B. Liu, D. Kong, Y. Wang, H. Y. Yang, *Energy Storage Mater.* **2018**, *10*, 92.
- [32] Y. Idota, T. Kubota, A. Matsufuji, Y. Maekawa, T. Miyasaka, *Science* **1997**, *276*, 1395.
- [33] R. A. Huggins, *J. Power Sources* **1999**, *81*, 13.
- [34] H. Lee, J. Cho, *Nano Lett.* **2007**, *7*, 78.
- [35] J. Yang, M. Winter, J. O. Besenhard, *Solid State Ionics* **1996**, *90*, 281.
- [36] L. Y. Beaulieu, J. R. Dahn, *J. Electrochem. Soc.* **2000**, *147*, 3237.
- [37] L. Beaulieu, D. Larcher, R. A. Dunlap, J. R. Dahn, *J. Alloys Compd.* **2000**, *297*, 122.
- [38] H. Sakaguchi, H. Honda, Y. Akasaka, T. Esaka, *J. Power Sources* **2003**, *119*, 50.
- [39] X. L. Wang, W. Q. Han, J. Chen, J. Graetz, *ACS Appl. Mater. Interfaces* **2010**, *2*, 1548.
- [40] X. L. Wang, M. Feygenson, H. Chen, C. H. Lin, W. Ku, J. Bai, M. C. Aronson, T. A. Tyson, W. Q. Han, *J. Am. Chem. Soc.* **2011**, *133*, 11213.
- [41] P. P. Ferguson, M. Rajora, R. A. Dunlap, J. R. Dahn, *J. Electrochem. Soc.* **2009**, *204*.
- [42] P. P. Ferguson, P. Liao, R. A. Dunlap, J. R. Dahn, *J. Electrochem. Soc.* **2009**, *13*.
- [43] A. D. W. Todd, P. P. Ferguson, J. G. Barker, M. D. Fleischauer, J. R. Dahn, *J. Electrochem. Soc.* **2009**, *1034*.
- [44] P. P. Ferguson, A. D. W. Todd, J. R. Dahn, *Electrochim. Commun.* **2008**, *10*, 25.
- [45] P. P. Ferguson, M. D. Fleischauer, J. M. Laforge, A. D. W. Todd, P. Li, J. R. Dahn, *J. Alloys Compd.* **2012**, *541*, 168.
- [46] C. J. Liu, F. H. Xue, H. Huang, X. H. Yu, C. J. Xie, M. S. Shi, G. Z. Cao, Y. G. Jung, X. L. Dong, *Electrochim. Acta* **2014**, *129*, 93.
- [47] O. Mao, J. R. Dahn, R. A. Dunlap, J. R. Dahn, *J. Electrochim. Soc.* **1999**, *146*, 414.
- [48] O. Mao, R. A. Dunlap, J. R. Dahn, *Solid State Ionics* **1999**, *118*, 99.

- [49] H. Y. Lee, S. W. Jang, S. M. Lee, S. J. Lee, H. K. Baik, *J. Power Sources* **2002**, *112*, 8.
- [50] Q. F. Dong, C. Z. Wu, M. G. Jin, Z. C. Huang, M. S. Zheng, J. K. You, Z. G. Lin, *Solid State Ionics* **2004**, *167*, 49.
- [51] S. Naille, F. Robert, F. Morato, P. Lippens, *J. Power Sources* **2007**, *174*, 1091.
- [52] J. Hassoun, G. Mulas, S. Panero, B. Scrosati, *Electrochem. Commun.* **2007**, *9*, 2075.
- [53] P. P. Ferguson, D. Le, A. D. W. Todd, M. L. Martine, S. Trussler, M. N. Obrovac, J. R. Dahn, *J. Alloys Compd.* **2014**, *595*, 138.
- [54] C. Q. Zhang, J. P. Tu, X. H. Huang, Y. F. Yuan, S. F. Wang, F. Mao, *J. Alloys Compd.* **2008**, *457*, 81.
- [55] R. Zhang, S. Upadhyay, M. Stanley Whittingham, *J. Electrochem. Soc.* **2011**, *158*, A1498.
- [56] Z. Dong, R. Zhang, D. Ji, N. A. Chernova, K. Karki, S. Sallis, L. Piper, M. Stanley Whittingham, *Adv. Sci.* **2016**, *3*, 1500229.
- [57] H. Shi, A. Zhang, X. Zhang, H. Yin, S. Wang, Y. Tang, Y. Zhou, P. Wu, *Nanoscale* **2018**, *10*, 4962.
- [58] H. Shi, Z. Fang, X. Zhang, F. Li, Y. Tang, Y. Zhou, P. Wu, G. Yu, *Nano Lett.* **2018**, *18*, 3193.
- [59] D. G. Kim, H. Kim, H. Sohn, T. Kang, *J. Power Sources* **2002**, *104*, 221.
- [60] N. Tamura, R. Ohshita, M. Fujimoto, S. Fujitani, M. Kamino, I. Yonezu, *J. Power Sources* **2002**, *107*, 48.
- [61] W. Pu, X. He, J. Ren, C. Wan, C. Jiang, *Electrochim. Acta* **2005**, *50*, 4140.
- [62] B. H. Shin, M. Liu, *Adv. Funct. Mater.* **2005**, 582.
- [63] J. Chen, L. Yang, S. Fang, S. I. Hirano, *J. Power Sources* **2012**, *209*, 204.
- [64] F. S. Ke, L. Huang, J. S. Cai, S. G. Sun, *Electrochim. Acta* **2007**, *52*, 6741.
- [65] F. Ke, L. Huang, H. Jiang, H. Wei, F. Yang, S. Sun, *Electrochem. Commun.* **2007**, *9*, 228.
- [66] K. Nishikawa, K. Dokko, K. Kinoshita, S. W. Woo, K. Kanamura, *J. Power Sources* **2009**, *189*, 726.
- [67] S. W. Woo, N. Okada, M. Kotobuki, K. Sasajima, H. Munakata, K. Kajihara, K. Kanamura, *Electrochim. Acta* **2010**, *55*, 8030.
- [68] F. Ke, L. Huang, H. Wei, J. Cai, X. Fan, F. Yang, S. Sun, *J. Power Sources* **2007**, *170*, 450.
- [69] X. M. Zheng, L. Huang, Y. Xiao, H. Su, G. L. Xu, F. Fu, J. T. Li, S. G. Sun, *Chem. Commun.* **2012**, *48*, 6854.
- [70] L. Xue, Z. Fu, Y. Yao, T. Huang, A. Yu, *Electrochim. Acta* **2010**, *55*, 7310.
- [71] L. Bazin, S. Mitra, P. L. Taberna, P. Poizot, M. Gressier, M. J. Menu, A. Barnabé, P. Simon, J. M. Tarascon, *J. Power Sources* **2009**, *188*, 578.
- [72] P. L. Taberna, S. Mitra, P. Poizot, P. Simon, J. M. Tarascon, *Nat. Mater.* **2006**, *5*, 567.
- [73] M. G. Kim, S. Sim, J. Cho, *Adv. Mater.* **2010**, *22*, 5154.
- [74] L. Nie, Y. Zhang, K. Ye, J. Han, Y. Wang, G. Rakesh, Y. Li, R. Xu, Q. Yan, Q. Zhang, *J. Mater. Chem. A* **2015**, *3*, 19410.
- [75] Y. Liu, M. Liu, D. Yin, W. Wei, P. N. Prasad, M. T. Swihart, *Chem. Mater.* **2017**, *29*, 3555.
- [76] J. Hassoun, S. Panero, B. Scrosati, *J. Power Sources* **2006**, *160*, 1336.
- [77] H. Mukaibo, T. Sumi, T. Yokoshima, T. Momma, *Electrochem. Solid-State Lett.* **2003**, 218.
- [78] H. Mukaibo, T. Momma, T. Osaka, *J. Power Sources* **2005**, *146*, 457.
- [79] B. J. Hassoun, S. Panero, P. Simon, P. L. Taberna, B. Scrosati, *Adv. Mater.* **2007**, *16*, 1632.
- [80] K. Zhuo, M. G. Jeong, C. H. Chung, *J. Power Sources* **2013**, *244*, 601.
- [81] H. Zhang, M. M. Zhang, M. M. Zhang, L. Zhang, A. Zhang, Y. Zhou, P. Wu, Y. Tang, *J. Colloid Interface Sci.* **2017**, *501*, 267.
- [82] J. Liu, Y. Wen, P. A. Van Aken, J. Maier, Y. Yu, *Nano Lett.* **2014**, *14*, 6387.
- [83] J. Liu, F. Liu, K. Gao, J. Wu, D. Xue, *J. Mater. Chem.* **2009**, *19*, 6073.
- [84] L. Huang, H. Wei, F. Ke, X. Fan, J. Li, S. Sun, *Electrochim. Acta* **2009**, *54*, 2693.
- [85] N. R. Shin, Y. M. Kang, M. S. Song, D. Y. Kim, H. S. Kwon, *J. Power Sources* **2009**, *186*, 201.
- [86] N. Tamura, M. Fujimoto, M. Kamino, S. Fujitani, *Electrochim. Acta* **2004**, *49*, 1949.
- [87] N. Tamura, Y. Kato, A. Mikami, M. Kamino, S. Matsuta, S. Fujitani, *J. Electrochem. Soc.* **2006**, *153*, A1626.
- [88] N. Tamura, Y. Kato, A. Mikami, M. Kamino, S. Matsuta, S. Fujitani, *J. Electrochem. Soc.* **2006**, *153*, A2227.
- [89] Z. Du, S. Zhang, *J. Phys. Chem. C* **2011**, *115*, 23603.
- [90] S. Zhang, Z. Du, R. Lin, T. Jiang, G. Liu, X. Wu, D. Weng, *Adv. Mater.* **2010**, *22*, 5378.
- [91] Sony Group Corporation, "Nexelion hybrid lithium ion batteries," can be found under <http://www.sony.net/SonyInfo/News/Press/200502/05-006E/>, 2005.
- [92] J. R. Dahn, S. Trussler, T. D. Hatchard, A. Bonakdarpour, K. C. Hewitt, M. Fleischauer, *Chem. Mater.* **2002**, *14*, 3519.
- [93] S. D. Beattie, J. R. Dahn, *J. Electrochem. Soc.* **2005**, *152*, C549.
- [94] A. D. W. Todd, R. E. Mar, J. R. Dahn, *J. Electrochem. Soc.* **2006**, *153*, 1998.
- [95] A. D. W. Todd, R. E. Mar, J. R. Dahn, *J. Electrochem. Soc.* **2007**, *154*, A597.
- [96] J. R. Dahn, R. E. Mar, A. Abouzeid, *J. Electrochem. Soc.* **2006**, *153*, 361.
- [97] P. P. Ferguson, M. L. Martine, A. E. George, J. R. Dahn, *J. Power Sources* **2009**, *194*, 794.
- [98] B. O. Jang, S. H. Park, W. J. Lee, *J. Alloys Compd.* **2013**, *574*, 325.
- [99] X. Shi, H. Song, A. Li, X. Chen, J. Zhou, Z. Ma, *J. Mater. Chem. A* **2017**, *5*, 5873.
- [100] J. Yang, J. Zhang, X. Zhou, Y. Ren, M. Jiang, J. Tang, *ACS Appl. Mater. Interfaces* **2018**, *10*, 35216.
- [101] B. T. Heligman, K. J. Kreder, A. Manthiram, *Joule* **2019**, *3*, 1051.
- [102] T. D. Hatchard, M. N. Obrovac, J. R. Dahn, *J. Electrochem. Soc.* **2006**, *153*, 282.
- [103] J. R. Dahn, R. E. Mar, M. D. Fleischauer, M. N. Obrovac, *J. Electrochem. Soc.* **2006**, *153*, 1211.
- [104] J. S. Thorne, R. J. Sanderson, J. N. Byers, J. R. Dahn, R. A. Dunlap, *J. Electrochem. Soc.* **2012**, *159*, A711.
- [105] Y. J. Kwon, J. Cho, *Chem. Commun.* **2008**, 1109.
- [106] H. Li, L. Shi, Q. Wang, L. Chen, X. Huang, *Solid State Ionics* **2002**, *148*, 247.
- [107] I. Rom, M. Wachtler, I. Papst, M. Schmied, *Solid State Ionics* **2001**, *139*, 329.
- [108] H. Mukaibo, T. Osaka, P. Reale, S. Panero, B. Scrosati, M. Wachtler, *J. Power Sources* **2004**, *132*, 225.
- [109] P. Nithyadharseni, B. Nalini, P. Saravanan, *Appl. Surf. Sci.* **2014**, *311*, 503.
- [110] P. Nithyadharseni, M. V. Reddy, B. Nalini, M. Kalpana, B. V. R. Chowdari, *Electrochim. Acta* **2015**, *161*, 261.
- [111] J. M. Lee, H. Jung, Y. Hwa, H. Kim, D. Im, S. G. Doo, H. J. Sohn, *J. Power Sources* **2010**, *195*, 5044.
- [112] J. M. Lee, W. S. Chang, B. C. Yu, H. Kim, D. Im, S. G. Doo, H. J. Sohn, *Electrochim. Commun.* **2010**, *12*, 928.
- [113] R. Verrelli, J. Hassoun, *J. Power Sources* **2015**, *299*, 611.
- [114] L. Ouyang, Z. Cao, H. Wang, R. Hu, M. Zhu, *J. Alloys Compd.* **2017**, *691*, 422.
- [115] H. Zhang, R. Hu, H. Liu, W. Sun, Z. Lu, J. Liu, L. Yang, Y. Zhang, M. Zhu, *J. Mater. Chem. A* **2016**, *4*, 10321.
- [116] Z. Xie, J. Zhao, Y. Wang, *Electrochim. Acta* **2015**, *174*, 1023.
- [117] M. Mao, F. Yan, C. Cui, J. Ma, M. Zhang, T. Wang, C. Wang, *Nano Lett.* **2017**, *17*, 3830.
- [118] F. Zhang, Y. Wang, W. Guo, S. Rao, P. Mao, *Chem. Eng. J.* **2019**, *360*, 1509.
- [119] F. Zhang, Y. Wang, W. Guo, P. Mao, S. Rao, P. Xiao, *J. Alloys Compd.* **2020**, *829*.
- [120] Y.-U. Kim, C. K. Lee, H.-J. Sohn, T. Kang, *J. Electrochem. Soc.* **2004**, *151*, A933.
- [121] A. Park, C. Park, *ACS Nano* **2017**, *11*, 6074.
- [122] H. Hwang, H. Kim, J. Cho, *Nano Lett.* **2011**, *11*, 4826.
- [123] D. Kong, H. He, Q. Song, B. Wang, W. Lv, Q.-H. Yang, L. Zhi, *Energy Environ. Sci.* **2014**, *7*, 3320.
- [124] J. Hassoun, G. Derrien, S. Panero, B. Scrosati, *Adv. Mater.* **2008**, *20*, 3169.
- [125] B. G. Derrien, J. Hassoun, S. Panero, B. Scrosati, *Adv. Mater.* **2007**, *19*, 2336.
- [126] G. X. Wang, J. H. Ahn, M. J. Lindsay, L. Sun, D. H. Bradhurst, S. X. Dou, H. K. Liu, *J. Power Sources* **2001**, *97–98*, 211.
- [127] M. Noh, Y. Kwon, H. Lee, J. Cho, Y. Kim, M. G. Kim, *Chem. Mater.* **2005**, *17*, 1926.
- [128] G. A. Elia, S. Panero, A. Savoini, B. Scrosati, J. Hassoun, *Electrochim. Acta* **2013**, *90*, 690.
- [129] R. Li, X. Sun, X. Zhou, M. Cai, X. Sun, *J. Phys. Chem. C* **2007**, *111*, 9130.
- [130] B. Guo, J. Shu, K. Tang, Y. Bai, Z. Wang, L. Chen, *J. Power Sources* **2008**, *177*, 205.
- [131] J. M. Chem, H. Liu, R. Hu, M. Zeng, J. Liu, M. Zhu, *J. Mater. Chem.* **2012**, *8022*.
- [132] Y. Wang, M. Wu, J. Zheng, J. Y. Lee, *Chem. Mater.* **2009**, *21*, 3210.
- [133] Y. J. Hong, Y. C. Kang, *Small* **2015**, *11*, 2157.
- [134] W. M. Zhang, J. S. Hu, Y. G. Guo, S. F. Zheng, L. S. Zhong, W. G. Song, L. J. Wan, *Adv. Mater.* **2008**, *20*, 1160.
- [135] S. Ding, W. Cheng, L. Zhang, G. Du, X. Hao, G. Nie, B. Xu, M. Zhang, Q. Su, C. A. Serra, *J. Colloid Interface Sci.* **2021**, *589*, 308.
- [136] S. Ding, W. Cheng, G. H. Du, Q. M. Su, L. J. Guo, X. J. Chen, S. Zhang, L. Shang, X. D. Hao, B. S. Xu, C. A. Serra, *Carbon* **2020**, *161*, 277.

- [137] B. Han, H. Mu, J. Chen, X. Hao, H. Wang, P. Liu, B. Xu, S. Ma, Y. Yang, T. Wang, S. Ding, C. A. Serra, G. Du, *Carbon* **2023**, *204*, 547.
- [138] S. Li, Z. Wang, J. Liu, L. Yang, Y. Guo, L. Cheng, M. Lei, W. Wang, *ACS Appl. Mater. Interfaces* **2016**, *8*, 19438.
- [139] H. Zhang, X. Huang, O. Noonan, L. Zhou, C. Yu, *Adv. Funct. Mater.* **2017**, *27*, 1606023.
- [140] X. Huang, S. Cui, J. Chang, P. B. Hallac, C. R. Fell, Y. Luo, B. Metz, J. Jiang, P. T. Hurley, J. Chen, *Angew. Chem. Int. Ed.* **2015**, *54*, 1490.
- [141] Y. Yu, L. Gu, C. Wang, A. Dhanabalan, P. A. Van Aken, J. Maier, *Angew. Chem. Int. Ed.* **2009**, *48*, 6485.
- [142] X. Zhou, L. Yu, X. Y. Yu, X. W. D. Lou, *Adv. Energy Mater.* **2016**, *6*, 1601177.
- [143] X. Li, A. Dhanabalan, L. Gu, C. Wang, *Adv. Energy Mater.* **2012**, *2*, 238.
- [144] Y. Guo, X. Zeng, Y. Zhang, Z. Dai, H. Fan, Y. Huang, W. Zhang, H. Zhang, J. Lu, F. Huo, Q. Yan, *ACS Appl. Mater. Interfaces* **2017**, *9*, 17172.
- [145] Y. Xu, Q. Liu, Y. Zhu, Y. Liu, A. Langrock, M. R. Zachariah, C. Wang, *Nano Lett.* **2013**, *13*, 470.
- [146] N. Zhang, Q. Zhao, X. Han, J. Yang, J. Chen, *Nanoscale* **2014**, *6*, 2827.
- [147] J. Guo, Z. Yang, L. A. Archer, *J. Mater. Chem. A* **2013**, *1*, 8710.
- [148] Z. Zhang, L. Yin, *Electrochim. Acta* **2016**, *212*, 594.
- [149] Y. Xu, J. Guo, C. Wang, *J. Mater. Chem.* **2012**, *22*, 9562.
- [150] Y. Liu, N. Zhang, L. Jiao, Z. Tao, J. Chen, *Nano Lett.* **2014**, *14*, 153.
- [151] Y. Li, C. Ou, J. Zhu, Z. Liu, J. Yu, W. Li, H. Zhang, Q. Zhang, Z. Guo, *Nano Lett.* **2020**, *20*, 2034.
- [152] L. Ji, Z. Tan, T. Kuykendall, E. J. An, Y. Fu, V. Battaglia, Y. Zhang, *Energy Environ. Sci.* **2011**, *4*, 3611.
- [153] B. Luo, B. Wang, X. Li, Y. Jia, M. Liang, L. Zhi, *Adv. Mater.* **2012**, *24*, 3538.
- [154] S. Chen, Y. Wang, H. Ahn, G. Wang, *J. Power Sources* **2012**, *216*, 22.
- [155] N. Li, H. Song, H. Cui, C. Wang, *Nano Energy* **2014**, *3*, 102.
- [156] J. Qin, C. He, N. Zhao, Z. Wang, C. Shi, E. Liu, J. Li, *ACS Nano* **2014**, *8*, 1728.
- [157] Y. Shen, T. Pan, L. Wang, Z. Ren, W. Zhang, F. Huo, *Adv. Mater.* **2021**, *33*, 2007442.
- [158] L. Jiao, J. Wang, H. L. Jiang, *Accounts Mater. Res.* **2021**, *2*, 327.
- [159] Q. Zhou, B. Jin, P. Zhao, S. Chu, R. Peng, *Chem. Eng. J.* **2021**, *419*, 129622.
- [160] A. S. Munn, P. W. Dunne, S. V. Y. Tang, E. H. Lester, *Chem. Commun.* **2015**, *51*, 12811.
- [161] Y. Pan, H. Li, X. X. Zhang, Z. Zhang, X. S. Tong, C. Z. Jia, B. Liu, C. Y. Sun, L. Y. Yang, G. J. Chen, *Chem. Eng. Sci.* **2015**, *137*, 504.
- [162] W. Sun, X. Zhai, L. Zhao, *Chem. Eng. J.* **2016**, *289*, 59.
- [163] T. Johnson, M. M. Łozińska, A. F. Orsi, P. A. Wright, S. Hindocha, S. Poulston, *Green Chem.* **2019**, *21*, 5665.
- [164] X. W. Zhang, M. Y. Lan, F. Wang, C. C. Wang, P. Wang, C. Ge, W. Liu, *Chem. Eng. J.* **2022**, *450*, 138082.
- [165] W. Luo, Y. Feng, D. Shen, J. Zhou, C. Gao, B. Lu, *ACS Appl. Mater. Interfaces* **2022**, *14*, 16379.
- [166] J. Shin, W. H. Ryu, K. S. Park, I. D. Kim, *ACS Nano* **2013**, *7*, 7330.
- [167] C. Yang, X. Liang, X. Ou, Q. Zhang, H. S. Zheng, F. Zheng, J. H. Wang, K. Huang, M. Liu, *Adv. Funct. Mater.* **2019**, *29*, 1807971.
- [168] G. Nie, Z. Huang, S. Ding, X. Hao, G. Suo, D. Han, Y. Xu, Y. Yang, W. Zhao, Q. Su, B. Xu, G. Du, C. A. Serra, *ACS Appl. Nano Mater.* **2022**, *5*, 2616.
- [169] M. Zhu, J. Wang, B. C. Holloway, R. A. Outlaw, X. Zhao, K. Hou, V. Shutthanandan, D. M. Manos, *Carbon* **2007**, *45*, 2229.
- [170] J. R. Miller, R. A. Outlaw, B. C. Holloway, *Science* **2010**, *329*, 1637.
- [171] Z. Y. Zhang, C. S. Lee, W. J. Zhang, *Adv. Energy Mater.* **2017**, *7*, 1.
- [172] S. Yoon, J. M. Lee, H. Kim, D. Im, S. G. Doo, H. J. Sohn, *Electrochim. Acta* **2009**, *54*, 2699.

Manuscript received: July 11, 2023

Revised manuscript received: August 17, 2023

Accepted manuscript online: August 23, 2023

Version of record online: September 6, 2023